Assimilation of Lightning Data Using a Nudging Method Involving Low-Level Warming

MAX R. MARCHAND AND HENRY E. FUELBERG

Florida State University, Tallahassee, Florida

(Manuscript received 24 February 2014, in final form 8 August 2014)

ABSTRACT

This study presents a new method for assimilating lightning data into numerical models that is suitable at convection-permitting scales. The authors utilized data from the Earth Networks Total Lightning Network at 9-km grid spacing to mimic the resolution of the Geostationary Lightning Mapper (GLM) that will be on the Geostationary Operational Environmental Satellite-R (GOES-R). The assimilation procedure utilizes the numerical Weather Research and Forecasting (WRF) Model. The method (denoted MU) warms the most unstable low levels of the atmosphere at locations where lightning was observed but deep convection was not simulated based on the absence of graupel. Simulation results are compared with those from a control simulation and a simulation employing the lightning assimilation method developed by Fierro et al. (denoted FO) that increases water vapor according to a nudging function that depends on the observed flash rate and simulated graupel mixing ratio. Results are presented for three severe storm days during 2011 and compared with hourly NCEP stage-IV precipitation observations. Compared to control simulations, both the MU and FO assimilation methods produce improved simulated precipitation fields during the assimilation period and a short time afterward based on subjective comparisons and objective statistical scores (~0.1, or 50%, improvement of equitable threat scores). The MU generally performs better at simulating isolated thunderstorms and other weakly forced deep convection, while FO performs better for the case having strong synoptic forcing. Results show that the newly developed MU method is a viable alternative to the FO method, exhibiting utility in producing thunderstorms where observed, and providing improved analyses at low computational cost.

1. Introduction

Lightning data provide an opportunity to locate areas of deep convection (e.g., Schultz et al. 2011; Rudlosky and Fuelberg 2013). With the scheduled launch of the Geostationary Operational Environmental Satellite-R (GOES-R) and its Geostationary Lightning Mapper (GLM) instrument in 2015 (Goodman et al. 2013), continuous lightning observations will be available over the continental United States and traditionally data-sparse regions of the Western Hemisphere. By assimilating observed lightning data into numerical weather prediction models, there is hope that forecasts can be improved.

Several procedures have been developed for assimilating observed data into numerical models. These include three-dimensional variational data assimilation (3DVAR; e.g., Hu et al. 2006; Xiao and Sun 2007), four-dimensional variational data assimilation (4DVAR; e.g., Mahfouf et al. 2005; Lopez 2011), ensemble Kalman filter (EnKF; e.g., Snyder and Zhang 2003; Dowell et al. 2011), and four-dimensional data assimilation (FDDA) nudging (e.g., Krishnamurti et al. 1991; Manobianco et al. 1994). Each of these methods utilizes an observation operator to translate model prognostic variables or control variables on the model grid to the observed data, or vice versa in the case of nudging.

A simple, yet accurate observation operator does not exist for lightning since it is produced by electrical fields that typically are not a model prognostic variable. Translating traditional model prognostic variables such as temperature or wind, or even less traditional variables such as graupel or vertical velocity, into an electric field requires a complex and nonlinear set of equations (e.g., Mansell et al. 2005; Kuhlman et al. 2006; Barthe and Pinty 2007; Fierro et al. 2008). However, nonlinear operators often prevent variational methods from producing the optimal analysis (Marecal and Mahfouf

Corresponding author address: Max R. Marchand, Florida State University, Earth, Ocean, and Atmospheric Science Meteorology, Rm. 404 Love Bldg., 1017 Academic Way, Tallahassee, FL 32306-4520.
E-mail: mrm06j@my.fsu.edu

DOI: 10.1175/MWR-D-14-00076.1

© 2014 American Meteorological Society

2003). Furthermore, adequately relating hydrometeors to thermodynamic parameters requires considering the time evolution of the model to assure dynamical consistency, making it difficult to successfully use 3DVAR. Although 4DVAR can consider the time evolution of a simulated storm when assimilating lightning data, the nonlinear moist physics that represents thunderstorms is difficult to properly linearize for constructing an adjoint model. Integrating a model backward with an inadequate adjoint model will yield a suboptimal analysis (Park and Zupanski 2003; Errico et al. 2007). An EnKF method of assimilating lightning observations is capable of modulating convection in a cloud-permitting application when using graupel volume as a proxy for lightning flash rates (Mansell 2014; Allen and Mansell 2013). However, the EnKF method is unable to initiate convection where all the ensemble members have a graupel volume of zero despite using a linear relationship between graupel volume and flash density. Consequently, at these locations the ensemble spread is zero and the EnKF and ensemble square root filter methods are prevented from increasing graupel volume where lightning is observed but none is simulated (Evensen 2003; Anderson 2001; Whitaker and Hamill 2002). However, this issue could be alleviated by perturbing the graupel mixing ratio and other model fields of the ensemble members near areas of observed lightning (e.g., Snyder and Zhang 2003; Dowell et al. 2004; Dowell and Wicker 2009). If the same observation operator from Mansell (2014) is used with a variational method, then a similar complication occurs. Where the first-guess graupel volume is zero, the Jacobian is zero and the variational method is unable to produce a storm where no graupel volume is simulated (Errico et al. 2007). When assimilating radar reflectivities to modify rainwater mixing ratios with the variational and EnKF methods, similar complications occur that are avoided when assimilating radar radial velocities. In summary, the complications of a potential lightning observation operator, as well as the processes that represent thunderstorms, have been obstacles to assimilating lightning data with the sophisticated variational or EnKF methods. Additionally, the computational cost of such sophisticated variational and EnKF methods applied at the horizontal scales needed to resolve thunderstorms is often impractical in an operational setting.

As a result of these difficulties, nudging is a viable alternative to the more sophisticated methods. Nudging methods have been used to assimilate lightning data because of their simple, computationally inexpensive way of producing convection while maintaining a dynamically consistent model solution. Many previous approaches have used latent heating and/or increasing the relative humidity as a proxy for observed lightning. These choices are well suited for coarse resolution and parameterized convection characterizing most of these applications, although they could also be applied at convective permitting scales. One of the first tests of lightning assimilation by nudging was simulating an extratropical cyclone (Alexander et al. 1999). Their effort was based on the work of Manobianco et al. (1994) and Jones and Macpherson (1997) who had used precipitation rates derived exclusively from polar-orbiting microwave and geostationary infrared imagery to either increase or decrease latent heating rates, and hence modulate convection. They also increased the relative humidity at levels where the latent heating rate had been increased. Alexander et al. (1999) found that including lightning data to derive rain rates used in modifying latent heating rates greatly improved the quality of simulated precipitation and pressure fields. This approach was further verified by Chang et al. (2001) using an alternative rainfall–flash rate relationship.

Pessi and Businger (2009b) also applied the latent heating nudging method of assimilating lightning data. They derived precipitation rates from a rainfall–flash rate relationship constructed using data from the precipitation radar on the Tropical Rainfall Measuring Mission (TRMM) satellite (Pessi and Businger 2009a). Simulated latent heating rates were not set to zero in locations where the model produced deep convective rainfall, but no lightning was observed since detection efficiencies and flash rates were small. A related latent heating–based diabatic digital filter initialization (DDFI) assimilation method currently is part of the Rapid Refresh (RAP) assimilation procedure (Weygandt et al. 2008). Since the procedure uses radar data and lightning data, convection can be suppressed only where radar data coverage is adequate.

Lightning data assimilation methods developed by Papadopoulos et al. (2005) and Mansell et al. (2007) enhanced convection by increasing humidity, not by increasing latent heating rates. These methods were based on techniques to assimilate radar reflectivity data by Gallus and Segal (2001) and Rogers et al. (2000). Papadopoulos et al. (2005) increased humidity by nudging a model utilizing a convective parameterization scheme (CPS). They nudged their model toward empirically derived specific humidity profiles at locations where lightning was observed, regardless of whether the model had produced convection. Convection was not suppressed (i.e., humidity not decreased) where the model produced deep convection but no lightning was observed. Mansell et al. (2007) also developed a lightning data assimilation method resembling the radar assimilation method of Rogers et al. (2000) that utilized a CPS to control

convection. Where observed lightning flash rates exceeded a certain threshold but deep model convection was not present, the method incrementally added moisture to the parcel source layer. Additionally, where the CPS indicated deep convection but no lightning was observed, all convective tendencies were set to zero.

Based on Fierro and Reisner (2011), Fierro et al. (2012) developed a nudging method, utilizing relative humidity as a proxy for assimilating lightning data, which was appropriate for convection permitting scales. They used total lightning data from the Earth Networks Total Lightning Network (ENTLN; http://earthnetworks.com/Products/TotalLightningNetwork.aspx) mapped on a 9-km grid to mimic that of the proposed GLM. At locations where lightning was observed, the water vapor in the mixed phase region (from 0° to −20°C) was increased as a hyperbolic tangent function of the simulated graupel mixing ratio and flash rate. The function increased water vapor less for greater graupel mixing ratios. Simulations produced precipitating convection that was better collocated with observed reflectivity fields than were control simulations. Fierro et al. (2014) compared results from their method with those from a 3DVAR assimilation of radar reflectivity during a derecho event. Their lightning assimilation method better forecast the location and intensity of the storm event. In addition, Lynn et al. (2014) noted that the method could improve lightning forecasts and also introduced an extension of the method to suppress spurious convection. A potential shortcoming of moistening to produce deep convection is that considerable water vapor may need to be added to the model, which would produce a moist bias in the humidity field. In simulations presented later from the finest domain, average precipitable water after 12 h of assimilation was 1.1%–2.1% greater than the control simulation not using the method. If hydrometeors and accumulated precipitation are included, values were 2.5%–3.6% greater.

The above studies illustrate how relative humidity can be increased to initialize deep convection and indirectly produce more accurate profiles of heating rate. In contrast, the current research develops and tests an alternative method of assimilating lightning data that is intended for convection permitting scales. Our method promotes convection by warming a layer instead of moistening it at those locations where lightning is observed but not simulated. Unlike previous methods that effectively warmed the mid- and upper troposphere by increasing latent heating and reduced CAPE, the current warming is prescribed in the updraft source layer so that CAPE is unaffected or increased. Our procedure to initiate or strengthen convective updrafts is conceptually similar to methods that primarily increased humidity. The objective is to modify the model temperature field just enough to produce storms in the correct location. The approach is based on the assumption that the model thermodynamic profiles are reasonably accurate and that the model merely needs a slight modification to initiate deep convection. Warming in the lower troposphere is hypothesized to conserve water vapor and to minimally modify the simulation to produce a better analysis and resulting forecast.

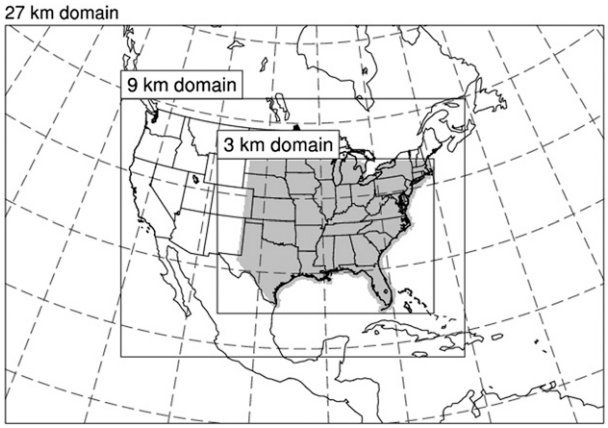

FIG. 1. Domains of the 27-, 9-, and 3-km horizontal grid spaced regions along with the precipitation verification domain (shaded gray) used in section 3.

2. Methodology

a. Model configuration and case studies

The fully compressible, nonhydrostatic Weather Research and Forecasting (WRF) Model with the Advanced Research dynamic solver (ARW, version 3.4.1; Skamarock and Klemp 2008) was used in this study. All simulations utilized adaptive time-stepping with two-way nesting between three domains (Fig. 1): an outer domain of 27-km horizontal grid spacing, an intermediate domain of 9-km spacing, and an inner domain of 3-km spacing, each with 60 vertical levels extending to the model top of 50 hPa. Assimilation was performed on the 9- and 3-km domains; no assimilation was performed on the outermost 27-km domain. Results presented in section 3 will focus on the 3-km domain. Simulations utilized the WRF single-moment 6-class bulk microphysics scheme (WSM6; Hong and Lim 2006), the Mellor–Yamada–Janjić turbulence kinetic energy planetary boundary layer scheme (MYJ-TKE; Janjić 1994), the Noah land surface model (Chen and Dudhia 2001; Ek et al. 2003), and Dudhia (1989) shortwave and Rapid Radiative Transfer Model longwave radiation schemes (RRTM; Mlawer et al. 1997; Iacono et al. 2000). The Kain–Fritsch CPS (KF; Kain and Fritsch 1993) was utilized on the outermost domain, while no CPS was utilized on either

the 9- or 3-km domains. This is similar to the Hu et al. (2006) cloud assimilation study that did not use CPS on their 9- and 3-km model grids because results from the nested 3-km domain became worse. In addition, simulations in Fierro et al. (2012) did not use a CPS on their 9-km model grid. We performed tests using the KF CPS on the 9-km domain and only minor changes occurred in the 3-km domain.

We ran simulations for three severe thunderstorm cases over the United States. The cases are 1) the outbreak of deadly supercell tornadoes on 27 April 2011 associated with strong large-scale forcing, 2) a squall line causing numerous severe wind reports across the Southeast on 15 June 2011 associated with more moderate forcing, and 3) 9 June 2011, a day of weaker forcing that produced a mixture of organized squall line features over the Northeast and Midwest and more isolated deep convection with numerous severe hail and wind reports across the southern Appalachians. These three days were among the most electrically active over the eastern United States during 2011.

All of the simulations included 6 h of model spinup between 0600 and 1200 UTC, after which lightning assimilation began and continued for 12 h. The simulations then were run an additional 12 h without assimilation, ending on 1200 UTC of the following day. The spinup period produced more realistic small-scale features in the model fields. And, by assimilating after the spinup period, our approach is more like the cycled data assimilation system commonly employed operationally (Kasahara et al. 1988), although experimental convection-permitting-scale forecasts that are employed operationally do not currently use cycling [e.g., High Resolution Rapid Refresh (HRRR), the National Centers for Environmental Prediction (NCEP) High-Resolution Window (HiResW), and the National Severe Storms Laboratory (NSSL) WRF]. The simulations employed in Mansell et al. (2007) and Fierro et al. (2012) also allowed model spinup before assimilating lightning data. We also performed tests without a spinup period, and our assimilation method affected simulations similarly whether or not the spinup period was used. Consequently, the tests without a spinup period are discussed only briefly in section 3d.

The 6-hourly 1° NCEP Final Operational Global Analysis (FNL) data were used as initial and lateral boundary conditions. Although simulations also were tested with 6-hourly 40-km North American Mesoscale Model (NAM) analyses (not shown), those employing FNL data generally produced better precipitation forecasts, both when assimilation was used and when it was not. In addition, the use of NAM analyses produced a wet precipitation bias while FNL analyses produced a relatively unbiased precipitation forecast.

b. *Lightning data*

We assimilated lightning observations from the ENTLN (http://earthnetworks.com/Products/TotalLightningNetwork.aspx). The ENTLN consists of a worldwide network of sensors that detects total lightning, i.e., both intracloud (IC) and cloud-to-ground (CG). In the 3-km model domain, the ENTLN's location uncertainty is less than 400 m, with the CG detection efficiency exceeding 95% over land. The IC detection efficiency is less, generally in the 50%–90% range [see Fig. 6 of Fierro et al. (2012)]. Each lightning flash was specified by its latitude, longitude, and time.

Before each model integration time step, the lightning flashes were binned and summed onto the 9-km domain grid that approximates the resolution of the upcoming GLM, similar to Fierro et al. (2012). If a flash was located within a model grid cell and occurred ±5 min of the current model time step, it was added to the count of that cell and time. For example, when the assimilation began at 1200 UTC and used a time step of 30 s, a flash occurring in a grid cell 1 s before 1200 UTC contributed to the flash count of the grid cell at 1200 UTC. After 10 model time steps the simulation time would be 1205 UTC, and since the flash occurred before the ±5-min window for that time, it would not contribute to the flash count of the cell at 1205 UTC. Thus, the flash count for each grid cell is effectively a flash rate density of integer values with units of flashes $(10\,\mathrm{min})^{-1}$ $(9\,\mathrm{km})^{-2}$. These units allowed each of the nine 3-km grid cells within the 9-km encompassing cell to be assigned the same flash rate density. Thus, flash rate densities from the 9-km domain grid were used when assimilating on the innermost 3-km domain as in Fierro et al. (2012). Although we computed these flash rate densities, our assimilation method does not depend on their magnitude, but only whether no flashes or one or more flashes occurred in the grid cell. This may erroneously force deep convection in stratiform regions of observed mesoscale convective systems where flash rates are low, but this is potentially alleviated by not performing assimilation where convection is simulated, as detailed in section 2e.

c. *Warming to initiate deep convection*

Our assimilation procedure is based on parcel theory that has well-known limitations (e.g., Markowski and Richardson 2010, 41–47). A parcel that is warmer than its environment is buoyant and may reach its level of free convection (LFC) to form a cloud. If the equilibrium level (EL) associated with the parcel is high enough and entrainment is not overly debilitating, a storm can develop. If the parcel is not warm enough to reach its LFC, or if the EL is too low to produce deep convection, parcel theory

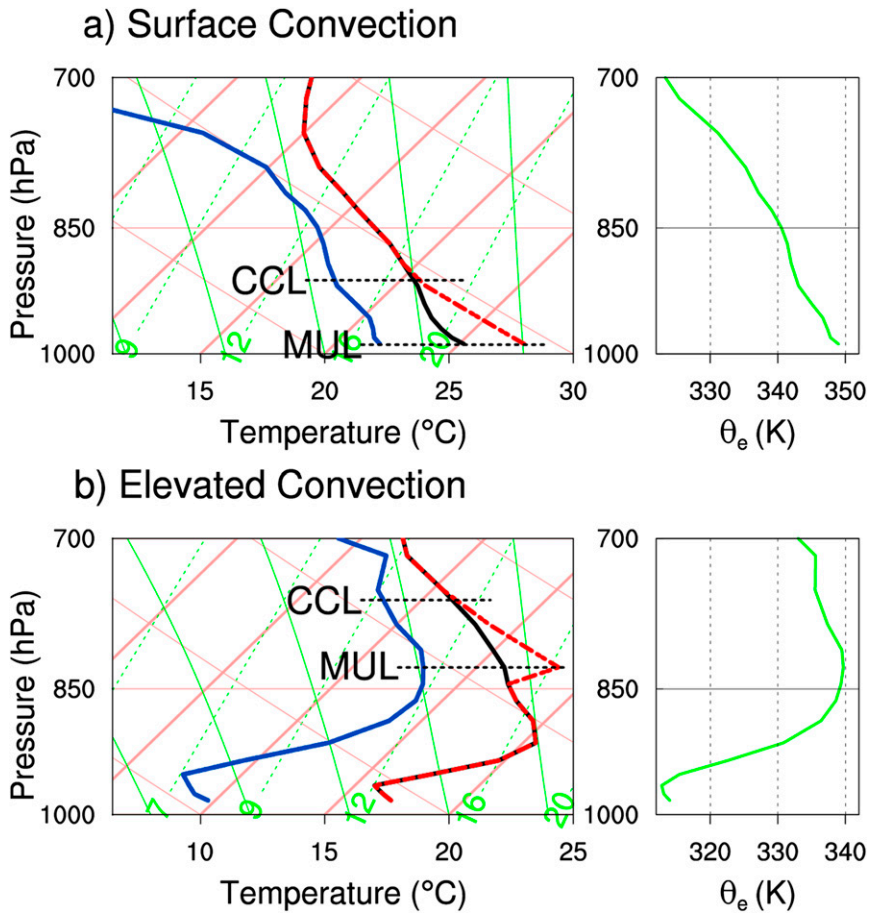

FIG. 2. Temperature profiles (red dashed lines) obtained from the MU method. Simulated temperatures are nudged toward this profile for a case with the most unstable level (MUL) at (a) the surface and (b) above the surface (near 830 hPa in this example). Also displayed are the preexisting temperature (black solid line) and the unmodified dewpoint temperature profile (blue solid line). On the right side are the preexisting equivalent potential temperature profiles (θ_e; green solid line) used to calculate the MUL for the respective cases.

indicates that it can be warmed in an effort to decrease the convective inhibition (CIN) below the LFC, raise the EL, and thereby increase the parcel's convective available potential energy (CAPE).

Warming near the surface to initiate convection is not a new concept. Cloud-scale simulations of deep convection frequently use a thermal perturbation or warm bubble to initialize storms (e.g., Klemp and Wilhelmson 1978; Lericos et al. 2007; Barthe et al. 2010). Because of its simplicity and effectiveness, the warm bubble approach is generally used in favor of other initiation methods such as modifying the model wind field (Loftus et al. 2008) or directly inserting an updraft (Naylor and Gilmore 2012).

Our nudging method warms the near-surface model profile to the convective temperature associated with the convective condensation level (CCL). This approach should help prevent more warming than necessary to create deep convection.

A convective temperature that is calculated from the surface-based CCL is not always appropriate since both surface-based and elevated convection occur in the atmosphere. To account for the possibility of elevated convection, the CCL and associated convective temperature were calculated from the most unstable level (MUL) of each grid cell's simulated sounding at each time step. The MUL is the altitude of maximum equivalent potential temperature and represents the level from which the most buoyant parcels will initiate. Figure 2 illustrates two hypothetical temperature profiles that the assimilation procedure would nudge toward: when the MUL is the surface (Fig. 2a), and when the MUL is above the surface (830 hPa in this example; Fig. 2b). Only model levels up to 700 hPa were considered in

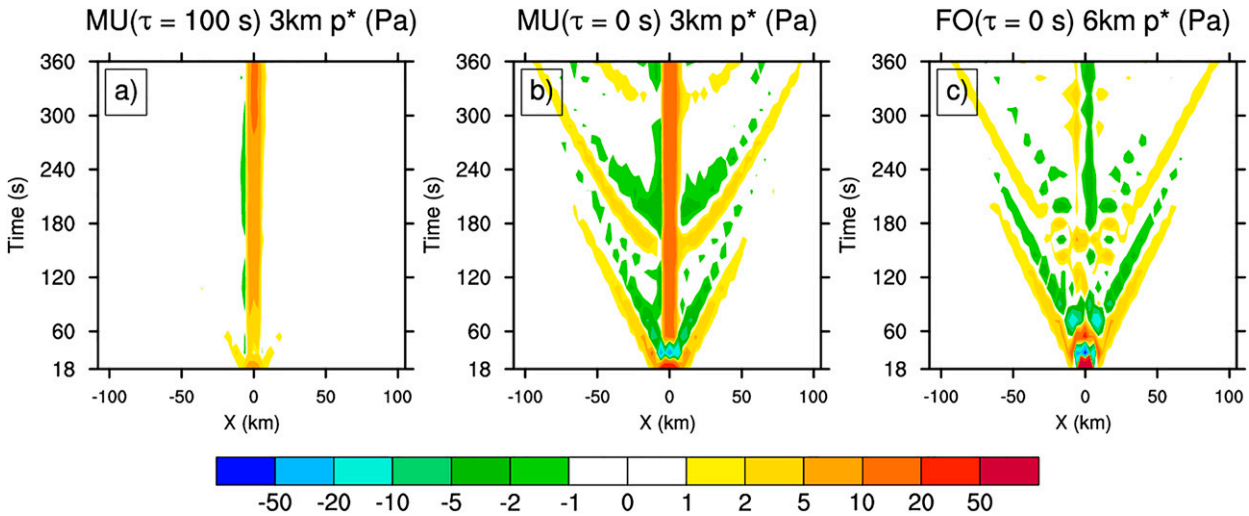

FIG. 3. Time evolution of pressure difference (shaded in Pa) between the control and simulations employing assimilation methods with different relaxation time scales (τ). The y axis is time (s), while the x axis is along an east–west line (km) away from the center point of assimilation. (a) MU using $\tau = 100$ s, (b) $\tau = 0$ s for MU, and (c) $\tau = 0$ s for FO. The altitude of the east–west axis is 3 km for MU and 6 km for FO, approximately corresponding to the level of maximum initial pressure perturbation at 18 s into the assimilation (i.e., after one time step). The 9 km × 9 km area of assimilation shown here is the same used in Figs. 5–8.

determining the MUL. Our assimilation method did not directly warm model levels below the MUL, but only at those levels between the MUL and CCL. Slight indirect warming typically occurred at the level immediately below the MUL because of diffusion and mixing. We did not constrain the amount of direct warming that could be performed. However, warming typically was less than 4 K and a common amount of warming at the MUL was approximately 2 K. Tests indicated that constraining the warming to 2 K or less did not degrade performance and would hypothetically help prevent numerical instabilities. Those test simulations are not presented here.

d. Newtonian nudging

Newtonian relaxation, or nudging (Anthes 1974), is a form of FDDA that is commonly used to incrementally modify model prognostic fields toward observed values at each model time step. How rapidly the field is modified depends on a nudging coefficient G of the general form:

$$d\alpha/dt = F + G \times (\alpha_o - \alpha), \quad (1)$$

where α is a prognostic variable, α_o is the observation associated with that variable, and F is the forcing term for the variable supplied by the model. Relatively small values of G produce more gradual modification that is associated with a larger e-folding time or relaxation time scale τ,

$$\tau = 1/G, \quad (2)$$

which helps limit dynamical imbalances that could cause an unstable solution.

In the method developed by Fierro et al. (2012, hereafter denoted FO), the desired humidity value is inserted during one time step so that τ is effectively 0. To examine the effect on a 9 km × 9 km area, we consider a location that is described later in section 3a. We also utilize a constant time step of 18 s on the 3-km grid domain as opposed to adaptive time stepping to enable a better comparison between the test simulations shown in Fig. 3. The increase of relative humidity by FO corresponds to a virtual temperature increase of ~0.3 K in the mixed-phase region near 6-km altitude. Our MU scheme produces a temperature increase of ~1.9 K at the MUL near 3-km height. However, whether implementing FO (Fig. 3c) or MU (Fig. 3b) with $\tau = 0$, both produce acoustic waves in the pressure fields that travel at 300–350 m s^{-1}. These pressure perturbations were computed by differencing the pressure fields at the selected heights (3 or 6 km) with those of a control simulation not using assimilation. Although the waves are the simulation's effort to remove hydrostatic imbalance, they represent unrealistic, high-frequency noise that have a small potential to cause unstable model solutions. They are similar to those found by Chagnon and Bannon (2005) when performing instantaneous warming in a linear model.

To remedy the undesirable waves, we ran test simulations using nudging coefficients of 5×10^{-3}, 0.01, 0.02, and 0.04 s^{-1}. Using MU with $G = 0.01$ s^{-1} ($\tau = 100$ s) limited the acoustic waves (Fig. 3a). A similar nudging

coefficient applied to FO likely would be beneficial; however, we kept our subsequent use of their approach as described in their paper. That is, $G = 0.01\,\mathrm{s}^{-1}$ was used only in the subsequent simulations employing MU. Although this value is large compared to synoptic scale values of $\sim 10^{-4}\,\mathrm{s}^{-1}$ (Stauffer and Seaman 1990), it is necessary since the time scale of thunderstorms is often less than 1 h. Finally, unlike many applications of nudging, we did not use a radius of influence due to the small spatial scales of thunderstorms. However, since the ENTLN lightning flashes were mapped onto the intermediate 9-km grid (see section 2b), the effective radius of influence is approximately 4.5 km.

e. *Denoting deep convection using maximum graupel mixing ratio*

If the ENTLN observations indicated lightning in a model grid cell, that cell was checked for the presence of simulated convection that was sufficiently intense to hypothetically produce the observed flashes. If the simulation suggested lightning at a grid cell where it was observed in nature, additional convection should not be induced by modifying the temperature profile. Thus, it was important to define a metric that is easily computed from the model variables and well correlated with lightning occurrence.

Noninductive charging is widely believed to be the primary mechanism causing thunderstorm electrification (e.g., Vonnegut 1963; Takahashi 1978; Saunders 1993). It occurs when there are collisions between graupel and ice crystals in the presence of supercooled water. For these collisions to occur, sufficiently strong vertical velocities must exist at temperatures less than 0°C. This explains the high correlation between lightning and updraft velocity (Price and Rind 1992; Pickering et al. 1998). If updrafts are sufficiently strong, graupel can be produced. As a result, graupel mass flux and vertically integrated ice mass are two metrics that have been associated with lightning flash rate (e.g., McCaul et al. 2009; Petersen et al. 2005; Deierling et al. 2008; Barthe et al. 2010). Unfortunately, vertical velocity, graupel mass, and vertically integrated ice mass depend on the model grid spacing being used. Use of graupel mass flux compounds the sensitivity issue since it is a product of both vertical velocity and graupel mass. Although vertically integrated ice mass is likely to be less sensitive to model grid spacing, our experience is that large values can occur in stratiform winter precipitation areas not containing lightning.

Because of graupel's association with lightning and its ease of computation, we selected maximum graupel mixing ratio in a grid column (qgmax) as the model-derived metric to denote deep convection. The metric was used to determine where and when our data assimilation method would be deployed. If qgmax exceeded a prescribed threshold and lightning was observed, no assimilation was performed. Several thresholds of qgmax were tested: 0.5, 1.0, 2.0, 4.0, 8.0 $\mathrm{g\,kg^{-1}}$, and ∞ (i.e., no threshold). Similar to the behavior of the nudging coefficient, greater values of the qgmax threshold produced larger areas of assimilation and warming that forced deep convection. Although the simulations were not very sensitive to the threshold, a qgmax threshold of 1.0 $\mathrm{g\,kg^{-1}}$ produced the best results (not shown) and was used for all simulations. Most simulated storms with maximum updrafts $\geq 10\,\mathrm{m\,s^{-1}}$ and extending above the freezing level will have graupel mixing ratios exceeding this value (e.g., Fierro et al. 2009; McFarquhar et al. 2006).

f. *Verification with NCEP stage-IV precipitation observations*

The simulated precipitation fields were verified against hourly precipitation from NCEP's stage-IV dataset (Lin and Mitchell 2005). Stage-IV data are derived from radar and rain gauge observations and benefit from human quality control at the National Weather Service River Forecast Centers. The 3-km simulated precipitation data were interpolated to the ~4-km stage-IV grid within the inner most domain. However, we verified the simulated precipitation only within a smaller domain (gray shading in Fig. 1) where the stage-IV data were over or near land and east of the Rocky Mountains where they become more reliable.

Our verifications utilized equitable threat score (ETS; Schaefer 1990) and probability of false detection (POFD) calculated from a standard 2×2 contingency table of forecast and observed binary (i.e., rain or no rain) hourly precipitation events that exceeded certain thresholds (Wilks 1995). Three precipitation thresholds were used: 1, 5, and 10 mm. The contingency table consists of hits a, false alarms b, misses c, and correct null events d that were used to calculate the metrics:

$$\mathrm{ETS} = \frac{a - a_{\mathrm{ref}}}{a + b + c - a_{\mathrm{ref}}}, \tag{3}$$

$$a_{\mathrm{ref}} = \frac{(a+b)(a+c)}{a+b+c+d}, \quad \text{and} \tag{4}$$

$$\mathrm{POFD} = \frac{b}{b+d}. \tag{5}$$

An ETS of 1.0 represents a perfect score, but values can be as small as $-1/3$, with negative values indicating a forecast whose skill is worse than a random forecast. Although ETS can overreward biased forecasts (Hamill 1999), it does so less than the critical success index or threat score (TS; Gandin and Murphy 1992; Baldwin and

Kain 2006). ETS differs from TS by including the a_{ref} term in (4), which represents the number of hits realized by chance. We used POFD in (5) to quantify overprediction since it represents the fraction of false alarm forecasts relative to the number of precipitation forecasts not exceeding a specified threshold.

A neighborhood spatial verification method, the fractions skill score (FSS; Roberts and Lean 2008), also was used. FSS penalizes small displacement errors of precipitation features less than ETS. This characteristic is particularly valuable when verifying simulations with small horizontal grid spacing. FSS, a variation of the fractions Brier score (FBS; Roberts 2005), provides leniency by defining a neighborhood region of cells that is centered on the grid cell of the verification domain. The simulated P_M and observed P_O fractions of grid cells located in the defined neighborhood that have precipitation amounts greater than a specified threshold are used to calculate FBS:

$$\mathrm{FBS} = \frac{1}{N}\sum_{i=1}^{N}[P_M(i) - P_O(i)]^2, \tag{6}$$

where N is the number of total grid cells in the verification domain. FBS ranges from 0 to 1, with 0 representing a perfect simulation. A deceptively small FBS can occur if there is only a small number of simulated and observed areas of rain exceeding the threshold, regardless of whether the grid cells with observed or simulated fractions greater than zero coincide. FSS provides a better comparison between different simulations or thresholds by dividing the FBS by a hypothetical worst case FBS ($\mathrm{FBS}_{\mathrm{worst}}$) from the given simulated and observed fractions:

$$\mathrm{FSS} = 1 - \frac{\mathrm{FBS}}{\mathrm{FBS}_{\mathrm{worst}}}, \tag{7}$$

where

$$\mathrm{FBS}_{\mathrm{worst}} = \frac{1}{N}\sum_{i=1}^{N}[P_M(i)^2 + P_O(i)^2]. \tag{8}$$

FSS defined in this way ranges from 0 to 1, with 1 representing a perfect simulation. Although biased forecasts generally are penalized by FSS, the exception is that the more biased forecasts sometimes yield better scores when the sample size and neighborhood area are small (Mittermaier and Roberts 2010).

Instead of using a square neighborhood to calculate FSS, we used a circular region with a specified radius as in Schwartz et al. (2009). The same precipitation thresholds were used as when calculating ETS. Six different radii of influence were used: 0, 20, 40, 60, 80, and 100 km. If the center of a surrounding grid cell was farther than the radius of influence, it was not considered to be in the neighborhood.

3. Results

We assessed the performance of the warming method of lightning assimilation using three simulations for each of the three severe storm cases: a control simulation (CT) without assimilation, a simulation using our MU method, and a simulation using the relative humidity nudging method described by FO. The FO method was chosen for comparison instead of other lightning nudging methods because they described its application at a convective permitting grid scale (3 km). We used the same constants as FO in their hyperbolic tangent function relating relative humidity to observed total lightning flash rate density and simulated graupel mixing ratio. However, our implementation of FO differs from theirs by updating the grid of lightning flash rates at each computational time step (adaptive step of ~10 s for the 3-km domain and ~30 s for the 9-km domain) instead of their 10-min interval. Fierro et al. (2012) also used a different spinup method, a shorter 2-h assimilation window, and a finer 1-km horizontal grid spacing than we used for their method here. However, the finest spacing Fierro et al. (2014) used was identical to ours: 3 km. The more frequent updating of lightning flashes in theory should aid the methods since deep convection is more accurately placed, although its effect on both methods likely is statistically insignificant. Additionally, the longer assimilation period allows both methods to influence the simulations more, and better mimics the cycling assimilation common in operational environments, albeit at coarser grid spacings, as described in section 2a. The following sections present results from the innermost 3-km domain of the various simulations.

a. Demonstrating the lightning assimilation methods

A fundamental test of lightning assimilation methods is whether they induce simulated deep convection in areas where lightning is observed. We used maximum column graupel mixing ratio (qgmax) exceeding 1 g kg^{-1} to identify locations of simulated deep convection. These locations were compared with locations of observed lightning flash rate densities (Fig. 4). As an example, Fig. 4 shows conditions after 6 h of assimilation for the 15 June squall-line case, a period of moderate forcing. The black shaded areas denote locations where simulated deep convection coincides with observed lightning. The top-left panel showing the CT simulation (Fig. 4a) contains few of these black regions that indicate

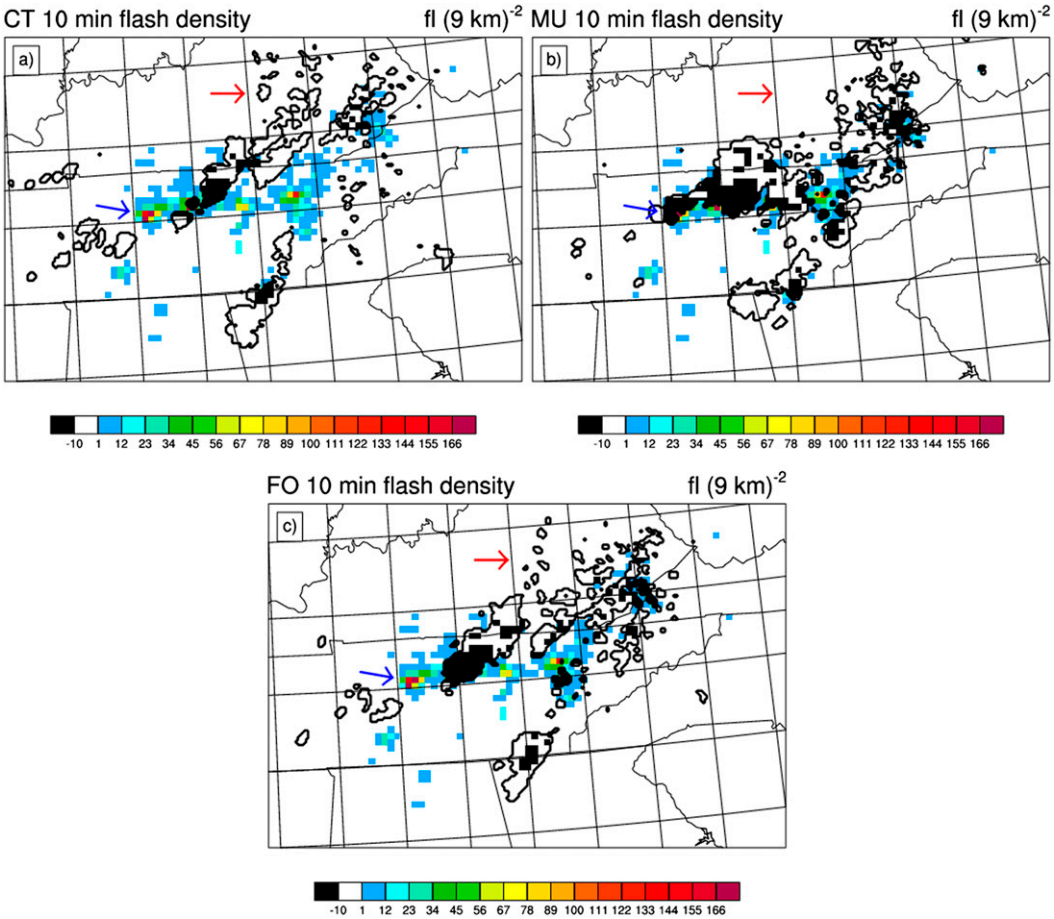

FIG. 4. Observed total lightning flash rate density over 10-min intervals [flashes (9 km)$^{-2}$, color shaded] with the 1 g kg^{-1} qgmax contour (in black) from the (a) CT, (b) MU, and (c) FO simulations at 1800 UTC 15 Jun 2011 (6 h after the start of assimilation). Black shading of flash rate density denotes areas where lightning is observed and simulated qgmax exceeds 1 g kg^{-1}, indicating agreement between deep simulated convection and observations. The hollow outlined regions denote regions of simulated deep convection where there is no corresponding observed lightning. See text for description of colored arrows.

agreement. Conversely, the MU and FO simulations (Figs. 4b,c) produce larger areas where simulated deep convection coincides with observed lightning. Comparing the MU and FO simulations, MU visually appears to exhibit somewhat better agreement. For example, FO does not produce deep convection in central Tennessee (blue arrows in Fig. 4) where total flash rate density exceeds 100 flashes (10 min)$^{-1}$ (9 km)$^{-2}$. FO better simulates this area 2 h later when the convection weakens and blends with other cells in the area. The hollow contours in Fig. 4 indicate regions of simulated deep convection where no lightning is occurring. The CT simulation exhibits more of these hollow contours and, hence more spurious simulated convection than MU in central and eastern Kentucky (red arrows in Fig. 4). Even though our method does not directly suppress convection, this reduction in spurious convection likely is a result of mesoscale subsidence (e.g., Fritsch and Chappell 1981) and better locating the storms early in their life cycles.

Simulations of a persistent, nearly stationary elevated thunderstorm in eastern North Carolina and South Carolina occurring near the start of assimilation at 1205 UTC 9 June 2011 further demonstrate the effectiveness of the two assimilation methods. The nearly stationary nature of the convection allows a single grid cell to capture the time evolution of the storm. Since it begins 5 min after the start of the 12-h assimilation period, the effects of past modifications by MU and FO are not present. The effects of the assimilation methods are easily seen by comparing soundings of the three simulations (Figs. 5 and 6).

At 5 min into the assimilations, MU has produced ~1.9 K of warming at the elevated MUL just above

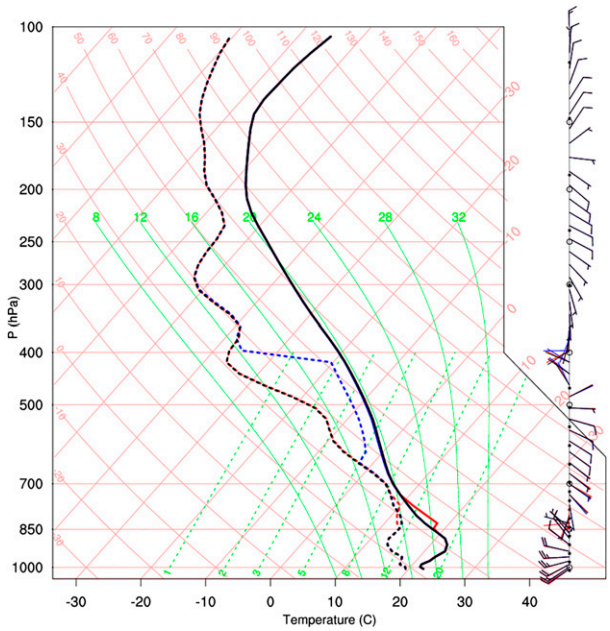

FIG. 5. Skew T–log$p$ diagram at 1205 UTC 9 Jun 2011 (5 min after the start of lightning assimilation) at the location of observed lightning in eastern North Carolina with air temperature (°C, solid lines), dewpoint temperature (°C, dashed line), and horizontal wind (kt, barbs along right axis, 1 kt = 0.5144 m s^{-1}). The different colored lines represent the different simulations: black for CT, red for MU, and blue for FO.

850 hPa (red lines in Figs. 5 and 6a). This causes enhanced buoyancy and a peak updraft of ~0.25 m s^{-1} above the layer warmed (Fig. 6c). This updraft has only a subtle effect on the dewpoint temperature (dotted red line in Fig. 5). As the updraft continues (not shown), saturation is achieved near and above the CCL (~750 hPa) that enables the available CAPE to be accessed. The storm develops slowly with a gradual increase in precipitable water (dashed red line in Fig. 7), composite reflectivity (solid red line in Fig. 7), and updraft speed reaching 11 m s^{-1} (not shown) 10–30 min after the start of assimilation. The result after 30 min of assimilation (1230 UTC; Fig. 8) is an approximately moist adiabatic profile in the saturated layer from the CCL to the cloud top at ~500 hPa that indicates a developing thunderstorm. Weather Surveillance Radar-1988 Doppler (WSR-88D) reflectivity observations from Raleigh, North Carolina, suggest that the approximately 750-hPa cloud base is realistic (not shown). The modifications due to assimilation that produce convection are small since a storm ~100 km away in the CT simulation has a nearly identical elevated cloud base and forms under similar thermodynamic conditions (not shown). The simulated storm before initiation has only slightly more conducive conditions, with mixing ratios ~1 g kg^{-1} greater between 700 and 750 hPa, which justifies the minimal modification performed by MU.

The MU performance for this storm may represent a relatively best case given the weak large-scale forcing that is commonly present for stationary storms. The MU certainly has deficiencies. For example, we observed cases (not shown) where the temperature of the MUL already equaled the convective temperature and consequently no modification was done even though convection had not begun. Simulated convection may have been absent in these situations because the mixing ratio decreased from the MUL to the CCL. Another situation that we sometimes observed was that the initial thermodynamic conditions appeared to be inaccurate. Consequently, a large amount of warming (4 K or more) was occasionally necessary to increase the MUL to the convective temperature and produce the observed deep convection. Even when the thermodynamic conditions are accurate, MU has a tendency to produce storms that are somewhat stronger than observed as seen by comparing the MU (solid red line) and observed reflectivity (solid gray line) in Fig. 7.

For the stationary storm example, the FO method increases midlevel relative humidity at the grid cell being considered, but no substantial convection occurs. At the start of assimilation (blue lines in Figs. 5 and 6b), the relative humidity between the 0° and −20°C levels increases from ~50% to ~85%, corresponding to a virtual temperature T_v increase of ~0.3 K (less than the 1.9 K observed for MU). This warming produces buoyancy and a peak updraft of ~0.2 m s^{-1} after 5 min, but approximately 200 hPa higher than does MU (Fig. 6c). Although this updraft is comparable to that from the MU simulation (red line of Fig. 6c), the FO-derived updraft is short lived since weak cooling of ~0.2 K (Fig. 6a) occurs in the mixed-phase region. This cooling weakens the updraft by counteracting the increase in T_v that was due to increasing the relative humidity. The MU also produces cooling (Fig. 6a), but it is much smaller than the warming. Additionally, some of the cooling occurs in the midlevels above the warmed layer, which results in a less convectively stable environment and deeper updraft. Thus, the FO updraft is confined to the midlevels and fails to saturate the low levels that would enable the convection to develop further. The FO's precipitable water increases only slightly after 30 min of assimilation (dashed blue line in Fig. 7) and then remains almost constant. The simulated composite reflectivity never exceeds 0 dBZ (solid blue line in Fig. 7). Thus, the low- to midlevels remain too dry, and precipitation never occurs at this and other nearby grid cells where lightning is observed.

Although the FO method often successfully initiates precipitating convection, its failure to do so in this

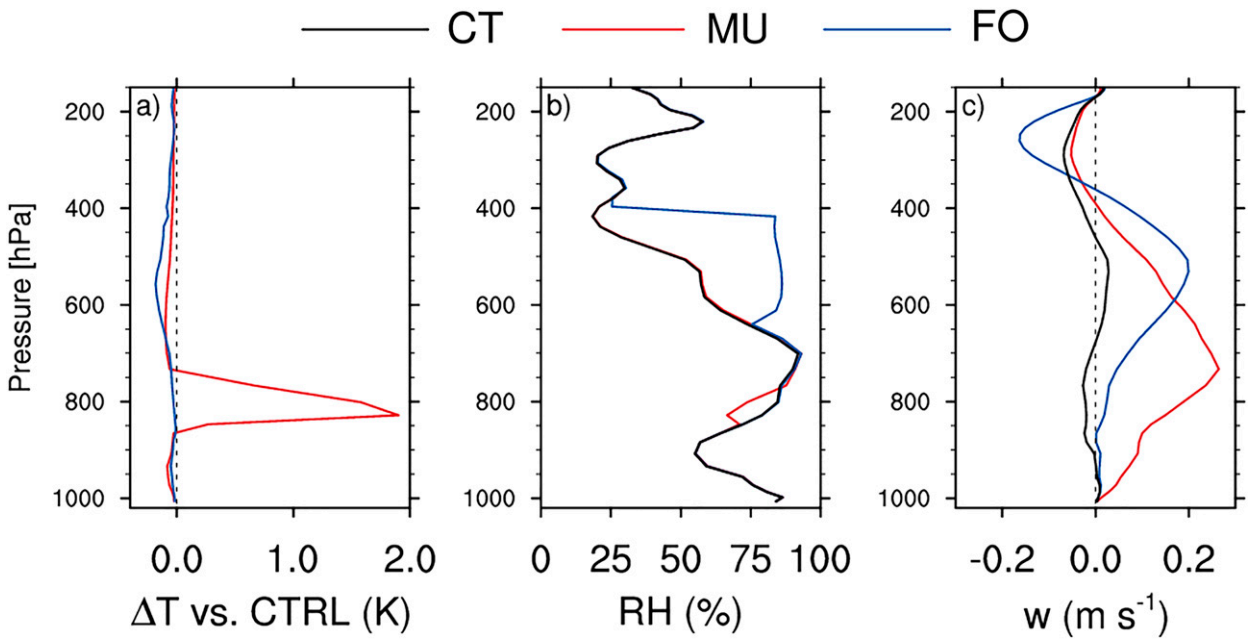

FIG. 6. Vertical profiles of (a) temperature difference (K) between lightning assimilation method and CT simulation, (b) relative humidity (%), and (c) vertical velocity ($m\,s^{-1}$) while utilizing the same line colors as in Fig. 5 and at the same time and location as in Fig. 5 (i.e., 1205 UTC 9 Jun 2011), 5 min after the start of lightning assimilation for a case of elevated convection.

example (Figs. 5–8) is not a rare occurrence. Sometimes its graupel mixing ratios exceed $1.0\,g\,kg^{-1}$, but no precipitation occurs at the surface. With no low-level updraft being induced, the area between convective cloud base and the mixed-phase region remains too dry (as in Fig. 8). If other forcing causes the atmosphere below the mixed-phase region to be conducive to low-level convection, then FO becomes effective at initiating deep convection. Later sections will show that both FO and MU are ineffective at some times in certain regions.

b. *Precipitation bias from lightning assimilation methods*

Hourly precipitation from both MU and FO averaged over all grid points in the verification domain (Fig. 1) is greater than from CT during the 12-h assimilation periods on all three study days (Fig. 9). However, after the assimilation period ends, both FO and MU overpredict precipitation for several hours followed by underprediction of precipitation in general by both methods. This is particularly apparent when one method greatly overpredicts precipitation during the assimilation period, such as the FO method on 27 April (Fig. 9a) and the MU method on 9 June (Fig. 9b). The underprediction results from excessive areas and amounts of deep convection and upper-level diabatic heating during assimilation that stabilize the atmosphere (not shown). These effects from the assimilation methods are an undesirable by-product since they can degrade forecast quality.

c. *Subjective verification of simulated precipitation fields*

A visual comparison between fields of simulated (MU and FO) and observed (ST4) hourly precipitation illustrates their performance and characteristics. This comparison is most useful at the last hour of the assimilation

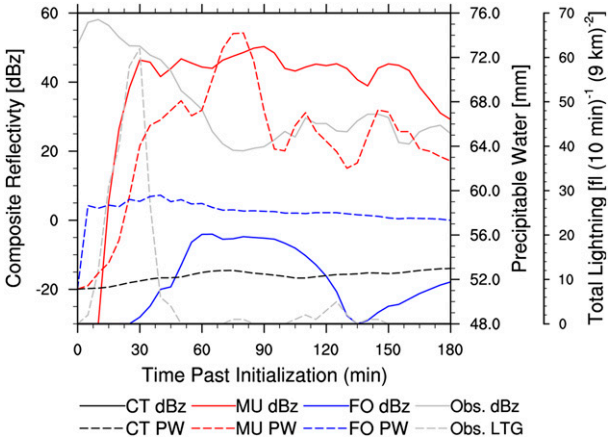

FIG. 7. Time series between 1200 and 1500 UTC 9 Jun 2011 of observed total lightning [flashes $(10\,min)^{-1}$ $(9\,km)^{-2}$, gray dashed line], observed composite reflectivity from WSR-88D at KRAX (dBZ, solid gray line), simulated composite reflectivity (dBZ, solid lines), and simulated precipitable water (mm, dashed lines) for CT, MU, and FO using the same line colors and location as Figs. 5–6. Note that the CT reflectivity is the minimum amount and, consequently, no solid black line is apparent in the figure.

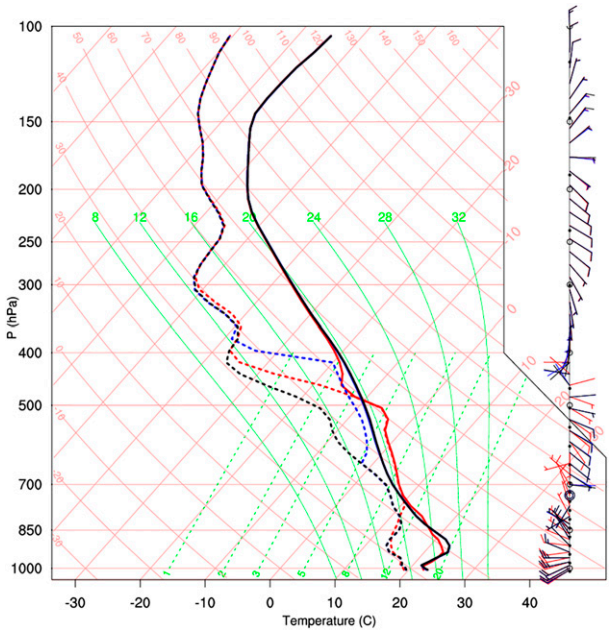

FIG. 8. As in Fig. 5, but at 1230 UTC 9 Jun 2011 (i.e., 30 min after the start of lightning assimilation).

period that ends at 0000 UTC (Figs. 10–12). Differences between the three runs typically are subtle, not ''eye catching.'' This visual evaluation is followed by a statistical comparison of the simulations with observations.

The 1-h accumulated precipitation of the CT simulation and ST4 observations on 27 April differ considerably at some locations (Fig. 10). Compared to the two June cases, this is a period of strong synoptic forcing. The CT produces precipitation in western Pennsylvania that is not observed in ST4 (blue arrows in Fig. 10). Although FO and MU produce a slightly smaller area of the spurious precipitation, MU places the feature too far south, while FO places it westward. The CT also incorrectly places large precipitation features in eastern Tennessee (red arrows) and west central Alabama (purple arrows). The FO better places these features, but its amounts greater than 40 mm exceed those of ST4. At these locations, MU erroneously produces features similar to CT. Near Washington, D.C., CT underpredicts precipitation relative to ST4. The FO behaves similar to CT, while MU reproduces the observed features near D.C., but with excessive precipitation amounts.

On 9 June with weak large-scale forcing, the CT precipitation pattern has numerous displacement errors relative to ST4 (Fig. 11). The CT too rapidly advances a squall line in the Northeast, leading to precipitation that is southeast of the observed (blue arrows in Fig. 11). The CT also displaces many of the small precipitation features in the Southeast, with little overlap between the observed and CT simulated features. The FO's precipitation features in the Northeast and Southeast appear similar to those from the CT, but with some greater precipitation amounts due to the increased humidity. The MU generally places many of the features in ST4, although both the areas and amounts of precipitation generally are too large. In central Kansas (red arrows), CT properly places the precipitation, but the amounts are too small. Nonetheless, both FO and MU produce amounts that better match ST4.

The CT simulation of the 15 June case generally reproduces many of the observed precipitation areas, but

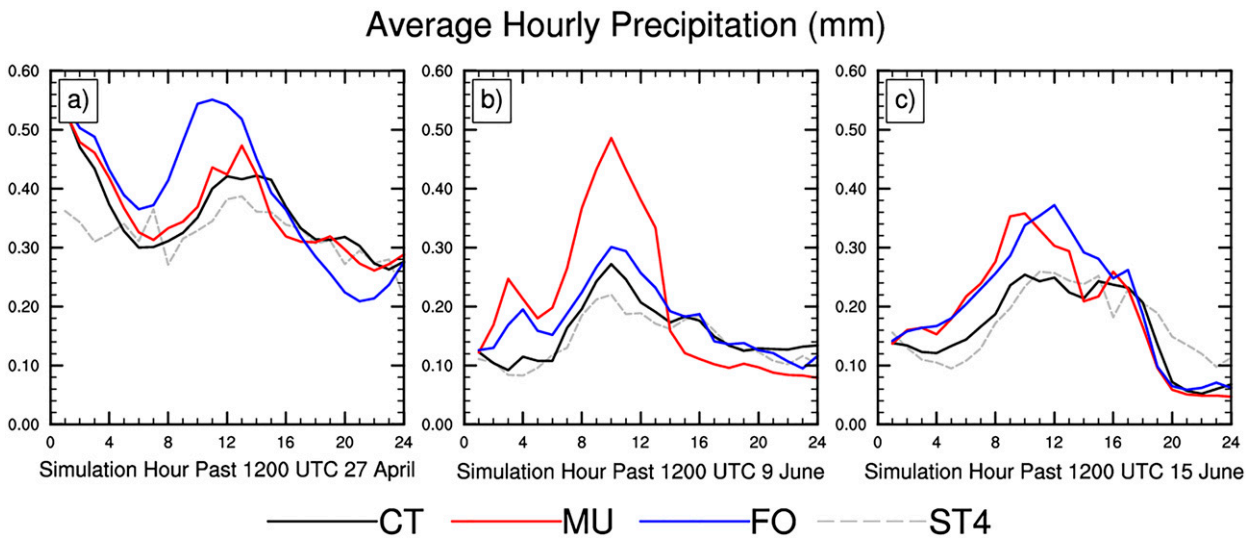

FIG. 9. Time series of hourly precipitation (mm) averaged over the verification domain (Fig. 1) for the first through last simulation hours on (a) 27 Apr, (b) 9 Jun, and (c) 15 Jun 2011 for the CT simulation (black line), MU simulation (red line), FO simulation (blue line), and stage-IV observations (ST4; gray dashed line). The assimilation ends at 12 h past 1200 UTC.

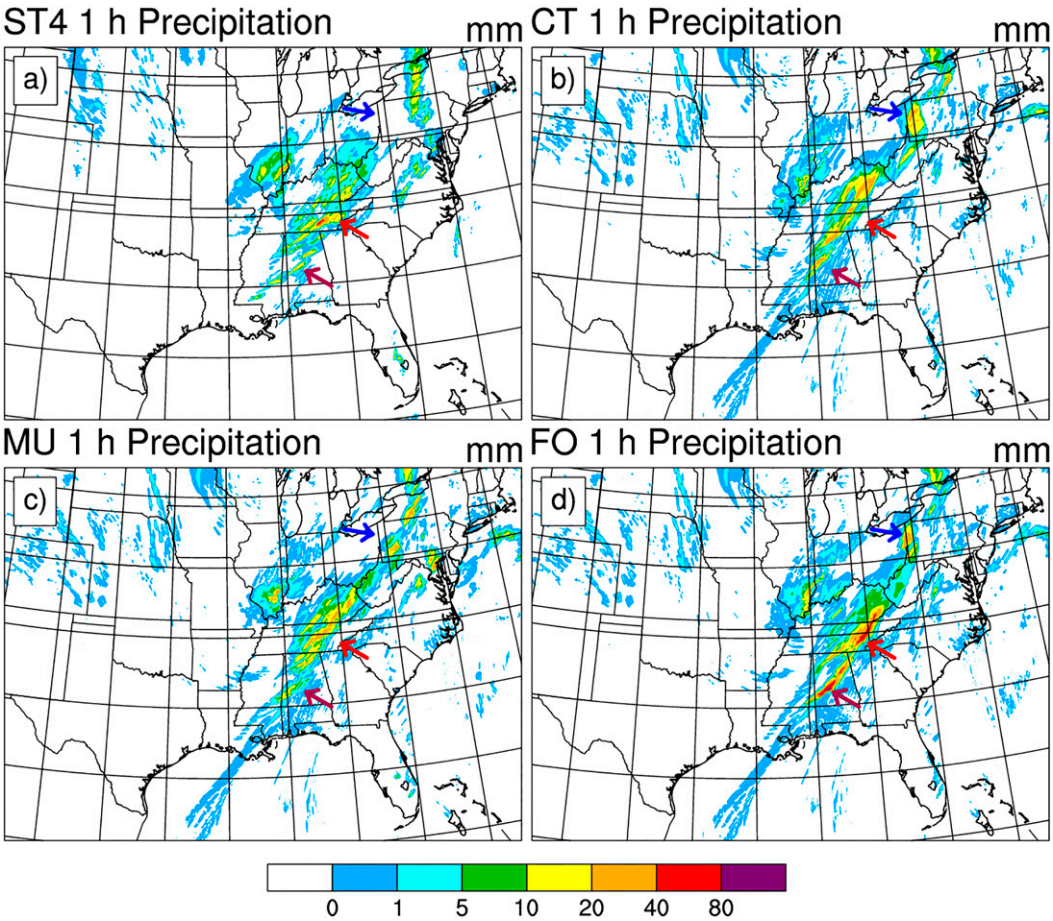

FIG. 10. Comparison of 1-h precipitation accumulation (mm) between 2300 UTC 27 Apr and 0000 UTC 28 Apr 2011 for (a) observed (ST4) and simulated sources: (b) CT, (c) MU, and (d) FO. See text for description of colored arrows.

many are displaced and exhibit erroneous amounts (Fig. 12). The CT places precipitation in southeastern Tennessee too far southwest, placing it into northeastern Alabama (blue arrows in Fig. 12). The FO displaces this feature much like CT, although with a larger area of light precipitation in southeastern Tennessee that is similar to the observed. Meanwhile MU better matches ST4 since it does not displace this feature to the southwest like FO and CT. However, MU does produce a larger area of intense precipitation than ST4. In western Kansas, CT produces an amount and area of precipitation that is smaller than observed (red arrows). Both MU and FO better place the precipitation and with improved intensity. The FO likely succeeds in simulating the Kansas convection because forcing already is present, as indicated by the small CT precipitation amounts in the same general area. The FO likely produces more favorable environmental conditions at the locations of observed lightning and, therefore, properly simulates the approximate placement and amount of precipitation. Similarly, MU initiates updrafts through low-level warming that eradicate inhibition where lightning is observed and allows deep convection appropriate for the simulated environment.

d. *Objective hourly precipitation scores*

The simulations can be evaluated quantitatively with the ST4 observations by computing objective precipitation scores for each hour, case, and using three precipitation thresholds (1, 5, and 10 mm). As before, we consider the 12-h assimilation period between 1200 and 0000 UTC. We also evaluate simulations that continue the assimilation for 12 additional hours ending at 1200 UTC (denoted MU24 and FO24). Including these longer runs will illustrate that results are improved if assimilation continues.

Certain generalizations about the ETS (Fig. 13) and FSS (Fig. 14) are applicable to all three study days. For example, MU and FO perform better than CT in terms of greater ETS and FSS during the 12-h assimilation

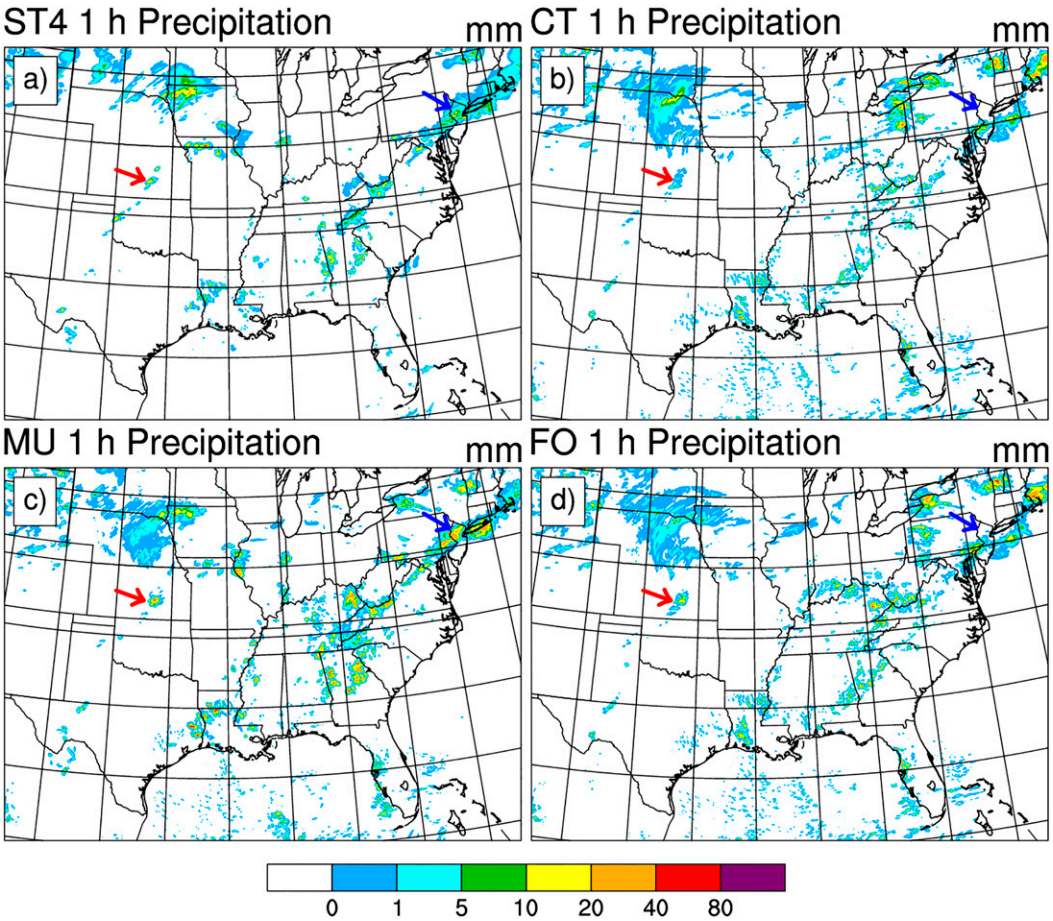

FIG. 11. As in Fig. 10, but between 2300 UTC 9 Jun and 0000 UTC 10 Jun 2011.

period at all three precipitation thresholds. After the 12-h assimilation period, MU and FO generally perform better than CT in terms of ETS and FSS during simulation hours 13–18 of the respective days. This improvement is more evident at the 1- and 5-mm thresholds than the 10-mm threshold since the latter are smaller in area and more prone to displacement errors. The improvement wanes with time, and neither assimilation method exhibits clear improvement during simulation hours 19–24. This diminishing model improvement is similar to that of previous radar assimilation studies (e.g., Hu et al. 2006; Wang et al. 2013) due to the short predictability of convective systems.

The MU produces consistently greater ETS and FSS than FO during the 9 June 12-h assimilation period with weak large-scale forcing (Figs. 13d–f and solid lines of Figs. 14d–f). The MU also scores better during the assimilation period on 15 June at both the 1- and 5-mm thresholds, while scores are similar at the 10-mm threshold. On 27 April when forcing is strong and MU has difficulty producing additional deep convection, FO typically performs better than MU in terms of ETS. When assessing FSS during the last 6 h of assimilation (ending with simulation hour 12), MU scores better than FO for the 5- and 10-mm thresholds at the larger radii of influence (x axis of Fig. 14). One should recall from section 2f that larger radii are not as likely to penalize large displacement errors. When the assimilation continues for 12 additional hours (dashed lines of Fig. 13), the MU24 simulation performs better and exhibits consistently greater ETS than the FO24 simulation for the 1- and 5-mm thresholds. For the 10-mm threshold, ETS become more ambiguous during the 27 April and 15 June cases.

When a spinup period as described in section 2a was not utilized, the ETS results are similar, with both assimilation methods performing better than CT during assimilation and during approximately the first 6 h of the forecast period. A large difference in ETS between initialization methods occurs during the 15 June case, as indicated by the CT ETS (black line) in Fig. 15 compared to that in Figs. 13g–i. The spinup period increases

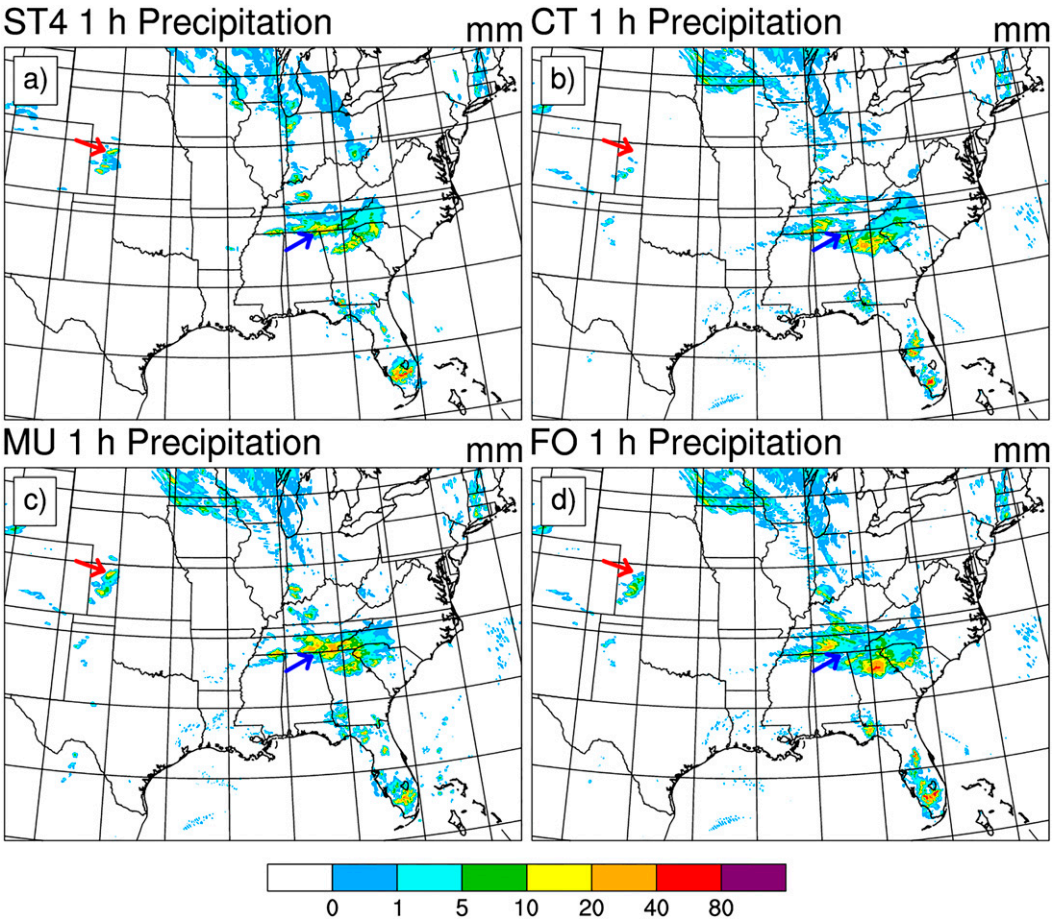

FIG. 12. As in Fig. 10, but between 2300 UTC 15 Jun and 0000 UTC 16 Jun 2011.

the ETS of CT considerably less during the other cases (not shown), except during the forecast period of the 9 June case. On these other two cases FO performs similarly with and without spinup in terms of ETS, while MU ETS increases modestly during the 27 April case.

We also experimented with bias correcting the ETS (Hamill 1999), but results did not seem advantageous relative to the uncorrected ETS (Fig. 13) and are not shown. During assimilation, bias-corrected ETS tend to be greater for the assimilation methods because the methods often overpredict precipitation where lightning is observed, particularly in the case of MU. Consequently, erroneous areas of precipitation would be corrected to smaller values that would increase ETS. Additionally, areas of overpredicted precipitation coinciding with areas of those observed would be corrected to more appropriate precipitation values that could also increase ETS. During the forecast period, bias correction has only a small effect on ETS because of less bias.

The probability of false detection (POFD) is a metric that indicates bias and the degree of agreement between locations of simulated and observed precipitation. A small value indicates that a simulation is not falsely producing many areas that exceed the threshold. Employing an overly active and biased lightning data assimilation method would produce a greater POFD relative to the CT simulation. At the 5- and 10-mm thresholds, the POFD of MU and FO is indeed consistently greater than that of CT during assimilation (Fig. 16). When considering the 1-mm threshold, however, the POFD for FO and MU sometimes is less than CT, even during assimilation. At this small 1-mm threshold, the MU simulations generally have a POFD less than that of FO. The smaller POFD for MU often results from it better locating a storm early in its life cycle and then properly propagating the storm.

4. Summary and conclusions

A new nudging method has been developed to assimilate lightning data into numerical models at convective-permitting scales. Our nudging method (denoted MU)

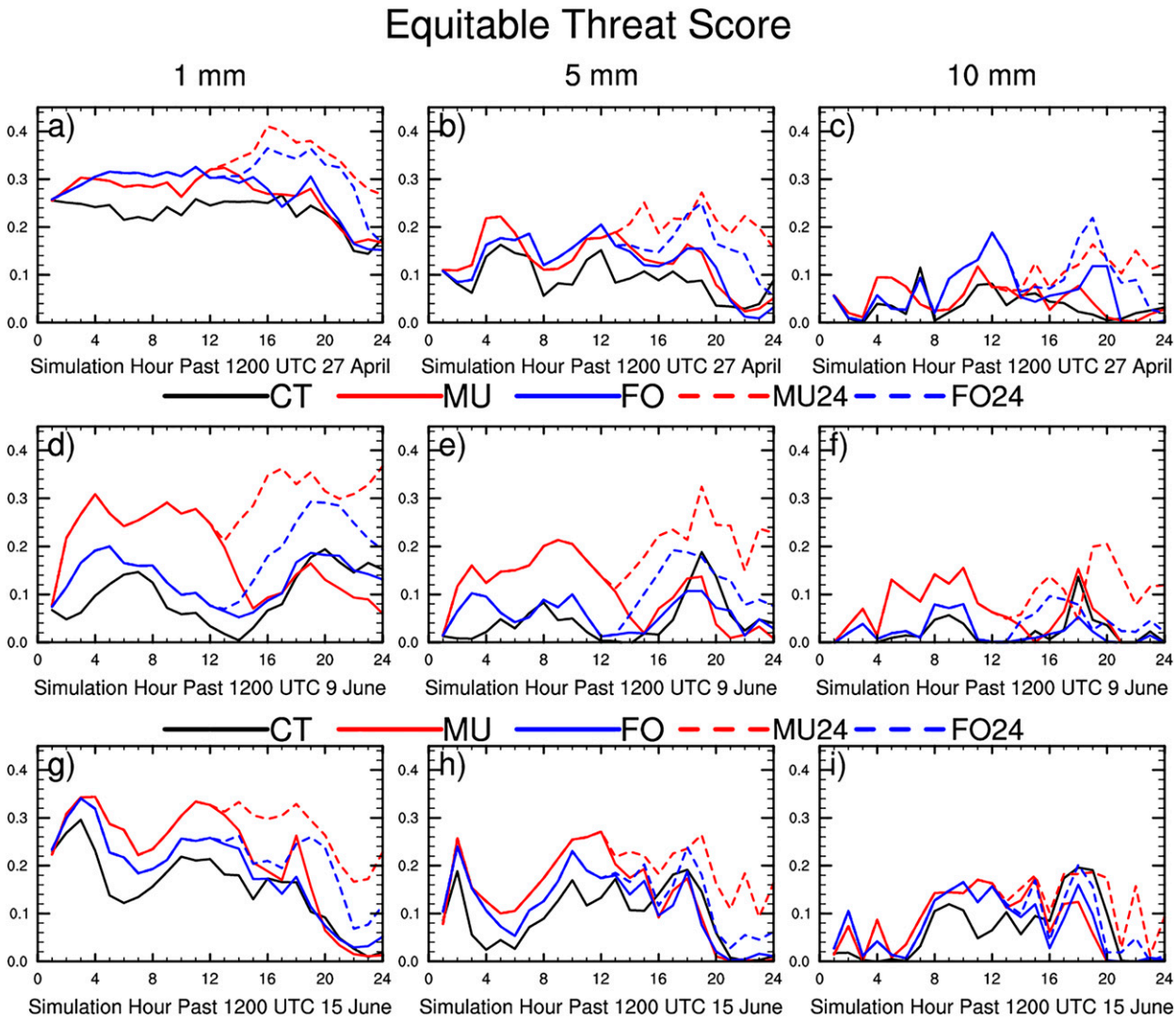

FIG. 13. Time series of hourly precipitation ETS relative to ST4 observations for five different simulations (CT in black, MU in solid red, FO in solid blue, MU24 in dashed red, and FO24 in dashed blue) and for three severe storm cases and three different precipitation thresholds: on 27 Apr using (a) 1-, (b) 5-, and (c) 10-mm thresholds; on 9 Jun using (d) 1-, (e) 5-, and (f) 10-mm thresholds; and on 15 Jun using (g) 1-, (h) 5-, and (i) 10-mm thresholds. The assimilation ends at 12 h past 1200 UTC for MU and FO, but continues throughout the MU24 and FO24 simulations. The 6-h spinup period before 1200 UTC is not considered.

warms the most unstable low levels of the simulated atmosphere at locations where lightning is observed but not simulated as diagnosed by the presence of graupel exceeding 1.0 g kg^{-1}. The objective is to initiate updrafts and deep convection in those locations. Observed total lightning data for method development were from the Earth Networks System. WRF simulations were performed across the central and eastern United States during three of the most electrically active days during 2011.

The results from our three cases indicate that neither the MU nor the Fierro et al. (2012) relative humidity nudging method is clearly superior in all cases. Instead, they show that the MU method is a viable alternative to FO. Based on equitable threat scores (ETS) and fraction skill scores using stage-IV precipitation observations, both the MU and FO methods improved simulated precipitation relative to control runs in which no assimilation was performed. The scores improved during assimilation and during a subsequent 12-h forecast period without assimilation, but only out to approximately 6 h. For the two June cases, MU improved ETS of the 1- and 5-mm precipitation amounts during the last hour of the assimilation period by more than 0.1 relative to the control. ETS improvement was smaller for the 10-mm amount and

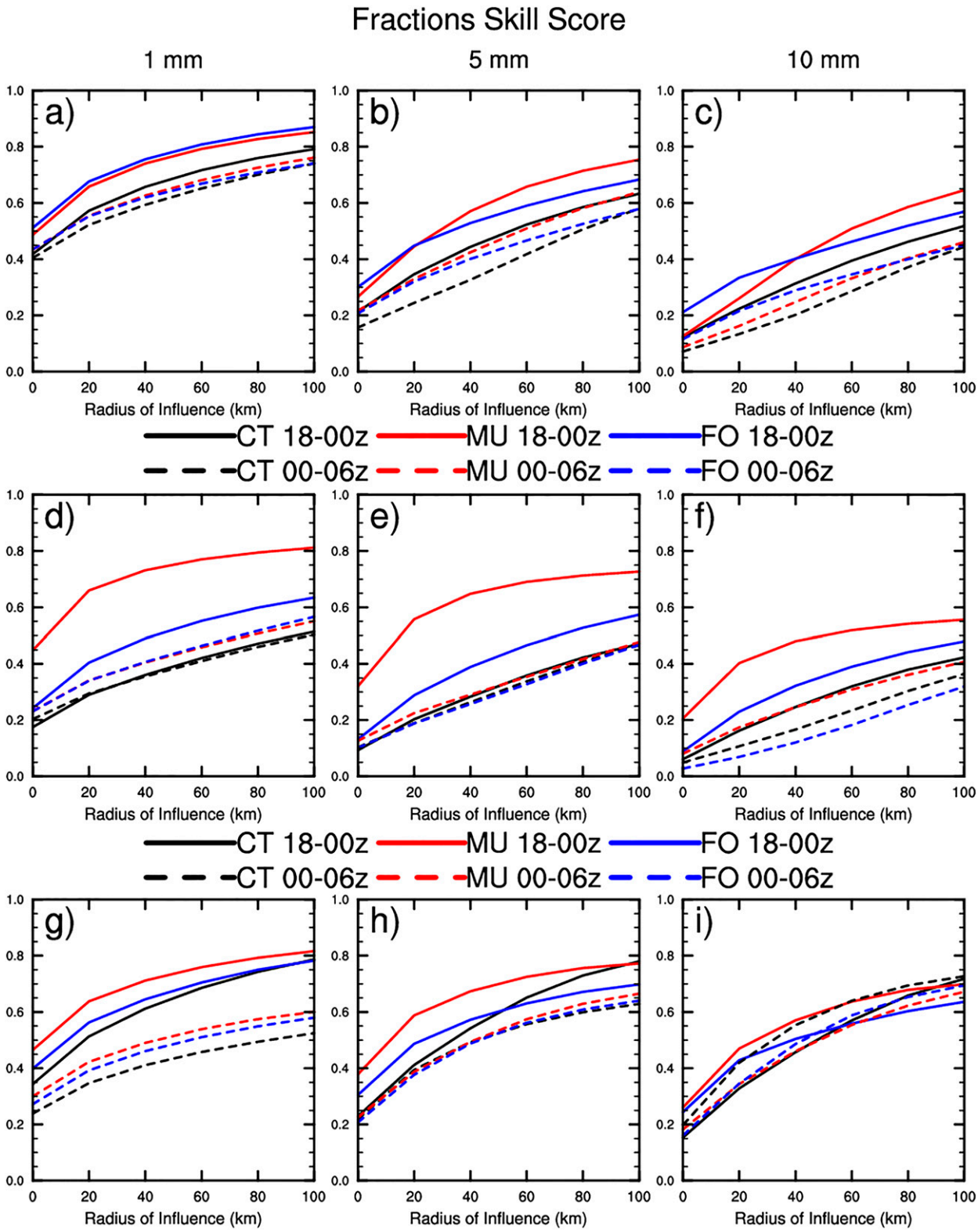

FIG. 14. FSS (y axis) averaged over the last 6 h of the assimilation period (1800–0000 UTC, solid lines) and over the nonassimilation period (0000–0600 UTC, dashed lines) using six radii of influence (km, x axis) for three severe storm cases and three different thresholds: on 27 Apr using (a) 1-, (b) 5-, and (c) 10-mm thresholds; on 9 Jun using (d) 1-, (e) 5-, and (f) 10-mm thresholds; and on 15 Jun using (g) 1-, (h) 5-, and (i) 10-mm thresholds.

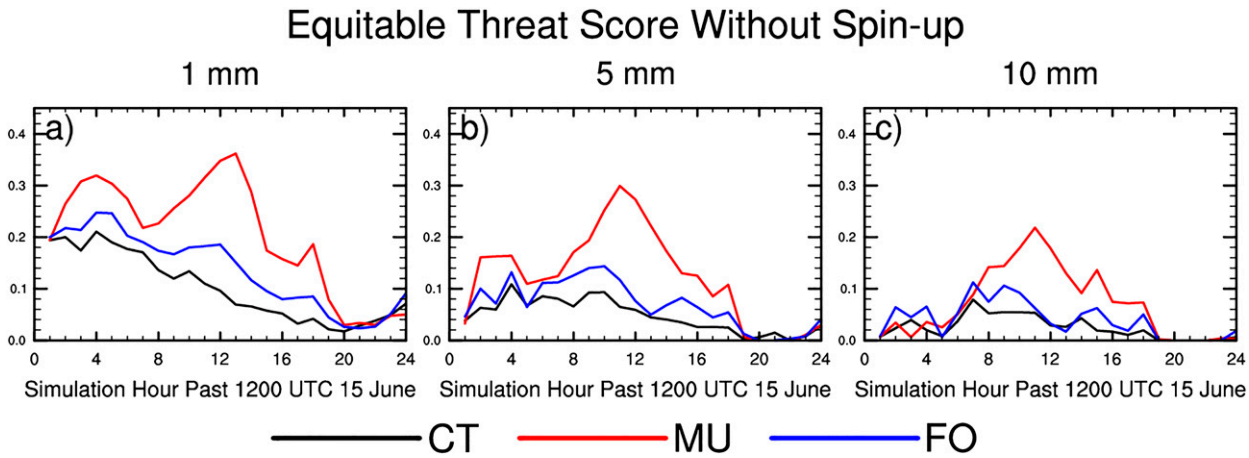

FIG. 15. As in Fig. 13, but without employing a 6-h spinup period (as described in section 2a) and only simulations CT, MU, and FO on 15 Jun using (a) 1-, (b) 5-, and (c) 10-mm thresholds.

27 April case. Meanwhile the FO method performed better for the 27 April case having strong synoptic forcing.

The FO method at times was more effective than MU at producing correctly located and appropriate amounts of precipitation. The MU method often proved more capable of producing deep convection in cases of observed isolated thunderstorms and storms with weak large-scale forcing. This increased effectiveness was a result of MU's ability to initiate an updraft in the low levels of the atmosphere that could force convection capable of overcoming the environmental convective inhibition (CIN). In contrast, the FO method added moisture in the 0° to −20°C mixed-phase region. The added moisture, by increasing the virtual temperature, enhanced buoyancy, but the resulting updraft often was confined to the midlevels. Consequently, the low levels near the convective cloud base sometimes would remain relatively dry. This dry layer often prevented parcels from becoming saturated, accessing CAPE, and eventually producing a thunderstorm. Although the greater humidity in the midlevels made deep convection more likely, without low-level forcing the FO method often could not produce a thunderstorm where one was observed. This important difference between MU and FO often allowed MU to perform considerably better than FO when CT failed to produce precipitating convection in a broad region where lightning is observed. Conversely, when low-level temperatures already are at the convective temperature as was common during the strongly forced 27 April case, MU often cannot initiate convection. Meanwhile, FO increased humidity and effectively initiated convection where it was observed. Combining the methods potentially would utilize the strengths of both methods and might further improve the simulations. The various parameters of FO's nudging function could also be tuned to produce better results since Fierro et al. (2012) applied those parameters only to high flash rate storms associated with a dryline over Oklahoma.

Both the FO and MU assimilation methods are employed at locations of observed lightning to produce or enhance convection that originally is not simulated. Neither method directly suppresses simulated convection where no lightning is observed. As a result, excessive areas and amounts of precipitation often occurred during assimilation. However, sometimes the procedures, particularly the MU method, indirectly suppressed the excessive areas of precipitation by better locating storms early in their life cycle and properly propagating them to the correct locations. This early overprediction, therefore, may be venial if the objective of assimilation is a better precipitation forecast since the wet precipitation bias disappears after the assimilation period. Still, the bias issue is relevant for producing additional forecast improvement since an underprediction of precipitation often occurred after the assimilation period produced a major overprediction of precipitation.

An assimilation method that directly suppresses convection in areas where lightning is not observed might diminish the current overprediction bias as well as moisture and temperature biases. However, developing such a method will be difficult since the absence of lightning does not preclude shallow warm rain convection. Furthermore, the absence of observed lightning at a location where it is simulated by the presence of graupel could indicate that either the atmosphere there actually is more stable than simulated, or that the

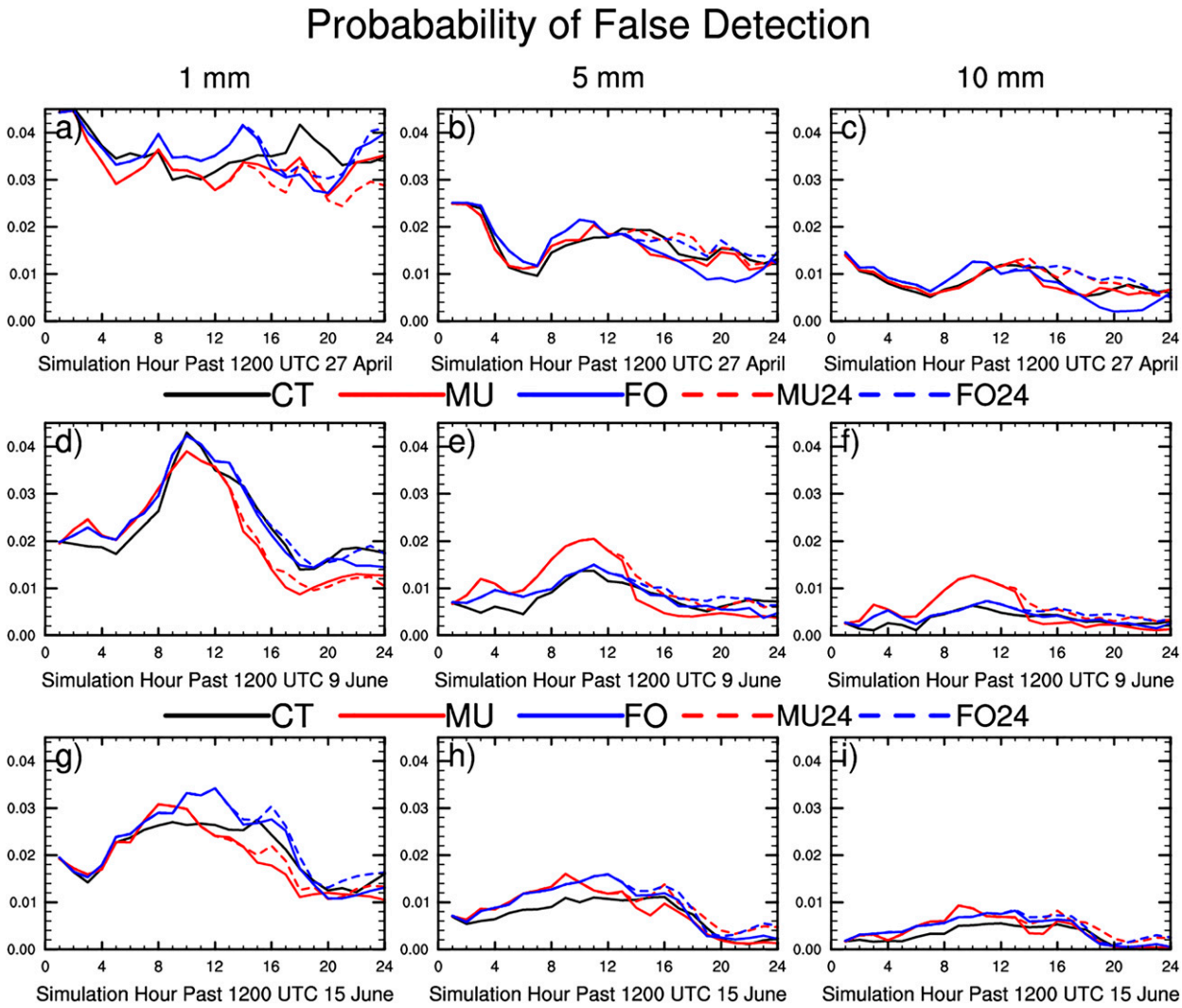

FIG. 16. As in Fig. 13, except for the probability of false detection (POFD).

atmosphere is conditionally unstable, but a trigger for deep convection has yet to occur. Effectively suppressing and modulating convection would necessitate additional atmospheric observations and/or more sophisticated, computationally expensive methods of assimilation.

Further improvements in lightning data assimilation likely will require more sophisticated methods. For example, the MU method has the potential to be implemented within the EnKF or 4DVAR assimilation schemes. Mansell (2014) and Allen and Mansell (2013) indicated that EnKF can modulate deep convection by considering the intensity of observed lightning and the corresponding simulated graupel content. However, both EnKF and 4DVAR often have difficulty assimilating lightning where no storm exists and lightning proxies such as graupel mixing ratio are zero. A first-guess field of zero simulated flashes produces a Jacobian of zero and no sensitivity to the observation (Errico et al. 2007) for variational methods. Meanwhile for EnKF, an ensemble with all first-guess fields of zero simulated flashes produces no ensemble spread (Evensen 2003; Anderson 2001). Consequently, without a supplementary method these sophisticated methods are unable to modify the analysis despite observations clearly indicating that it should do so. Since the MU method has a demonstrated ability to initiate convection, it could be employed to produce convection in the first-guess fields when running the model forward. With a nonzero Jacobian or ensemble spread, the sophisticated procedures could then successfully modulate convection.

Results from the Geostationary Lightning Mapper (GLM) represent a potential source of valuable

information about deep convection over the United States and regions of poor or no radar coverage. The preliminary results presented here indicate that our low-level warming nudging method is an effective and computationally inexpensive technique in which total lightning data can be assimilated into numerical weather models and thereby expand the utility of the GLM. However, we believe that considerable additional research will be needed before GLM data reach their full potential to improve forecasts by assimilation.

Acknowledgments. This research was sponsored by NOAA Grant NA10NES4400008 under the auspices of the Joint Center for Satellite Data Assimilation. We appreciate our many discussions with Dr. Michael Navon and Dr. Razvan Stefanescu of the Department of Scientific Computing at Florida State University.

REFERENCES

Alexander, G. D., J. A. Weinman, V. Karyampudi, W. S. Olson, and A. C. L. Lee, 1999: The effect of assimilating rain rates derived from satellites and lightning on forecasts of the 1993 Superstorm. *Mon. Wea. Rev.,* **127,** 1433–1457, doi:10.1175/1520-0493(1999)127<1433:TEOARR>2.0.CO;2.

Allen, B. J., and E. R. Mansell, 2013: Assimilation of pseudo Geostationary Lightning Mapper observations into a storm scale numerical model using the ensemble Kalman filter. *Sixth Conf. on the Meteorological Applications of Lightning Data,* Austin, TX, Amer. Meteor. Soc., 7.2. [Available online at https://ams.confex.com/ams/93Annual/webprogram/Paper223239.html.]

Anderson, J. L., 2001: An ensemble adjustment Kalman filter for data assimilation. *Mon. Wea. Rev.,* **129,** 2884–2903, doi:10.1175/1520-0493(2001)129<2884:AEAKFF>2.0.CO;2.

Anthes, R. A., 1974: Data assimilation and initialization of hurricane prediction model. *J. Atmos. Sci.,* **31,** 702–719, doi:10.1175/1520-0469(1974)031<0702:DAAIOH>2.0.CO;2.

Baldwin, M. E., and J. S. Kain, 2006: Sensitivity of several performance measures to displacement error, bias, and event frequency. *Wea. Forecasting,* **21,** 636–648, doi:10.1175/WAF933.1.

Barthe, C., and J.-P. Pinty, 2007: Simulation of a supercellular storm using a three-dimensional mesoscale model with an explicit lightning flash scheme. *J. Geophys. Res.,* **112,** D06210, doi:10.1029/2006JD007484.

——, W. Deierling, and M. C. Barth, 2010: Estimation of total lightning from various storm parameters: A cloud-resolving model study. *J. Geophys. Res.,* **115,** D24202, doi:10.1029/2010JD014405.

Chagnon, J. M., and P. R. Bannon, 2005: Wave response during hydrostatic and geostrophic adjustment. Part I: Transient dynamics. *J. Atmos. Sci.,* **62,** 1311–1329, doi:10.1175/JAS3283.1.

Chang, D.-E., J. A. Weinman, C. A. Morales, and W. S. Olson, 2001: The effect of spaceborne microwave and ground-based continuous lightning measurements on forecasts of the 1998 Groundhog Day storm. *Mon. Wea. Rev.,* **129,** 1809–1833, doi:10.1175/1520-0493(2001)129<1809:TEOSMA>2.0.CO;2.

Chen, F., and J. Dudhia, 2001: Coupling an advanced land surface–hydrology model with the Penn State–NCAR MM5 modeling system. Part I: Model implementation and sensitivity. *Mon. Wea. Rev.,* **129,** 569–585, doi:10.1175/1520-0493(2001)129<0569:CAALSH>2.0.CO;2.

Deierling, W., W. A. Petersen, J. Latham, S. Ellis, and H. J. Christian, 2008: The relationship between lightning activity and ice fluxes in thunderstorms. *J. Geophys. Res.,* **113,** D15210, doi:10.1029/2007JD009700.

Dowell, D. C., and L. J. Wicker, 2009: Additive noise for storm-scale ensemble data assimilation. *J. Atmos. Oceanic Technol.,* **26,** 911–927, doi:10.1175/2008JTECHA1156.1.

——, F. Zhang, L. J. Wicker, C. Snyder, and N. A. Crook, 2004: Wind and temperature retrievals in the 17 May 1981 Arcadia, Oklahoma, supercell: Ensemble Kalman filter experiments. *Mon. Wea. Rev.,* **132,** 1982–2005, doi:10.1175/1520-0493(2004)132<1982:WATRIT>2.0.CO;2.

——, L. J. Wicker, and C. Snyder, 2011: Ensemble Kalman filter assimilation of radar observations of the 8 May 2003 Oklahoma City supercell: Influences of reflectivity observations on storm-scale analyses. *Mon. Wea. Rev.,* **139,** 272–294, doi:10.1175/2010MWR3438.1.

Dudhia, J., 1989: Numerical study of convection observed during the Winter Monsoon Experiment using a mesoscale two-dimensional model. *J. Atmos. Sci.,* **46,** 3077–3107, doi:10.1175/1520-0469(1989)046<3077:NSOCOD>2.0.CO;2.

Ek, M. B., K. E. Mitchell, Y. Lin, E. Rogers, P. Grunmann, V. Koren, G. Gayno, and J. D. Tarpley, 2003: Implementation of Noah land surface model advances in the National Centers for Environmental Prediction operational mesoscale Eta model. *J. Geophys. Res.,* **108,** 8851, doi:10.1029/2002JD003296.

Errico, R. M., P. Bauer, and J.-F. Mahfouf, 2007: Issues regarding the assimilation of cloud and precipitation data. *J. Atmos. Sci.,* **64,** 3785–3798, doi:10.1175/2006JAS2044.1.

Evensen, G., 2003: The Ensemble Kalman Filter: Theoretical formulation and practical implementation. *Ocean Dyn.,* **53,** 343–367, doi:10.1007/s10236-003-0036-9.

Fierro, A. O., and J. M. Reisner, 2011: High-resolution simulation of the electrification and lightning of Hurricane Rita during the period of rapid intensification. *J. Atmos. Sci.,* **68,** 477–494, doi:10.1175/2010JAS3659.1.

——, L. M. Leslie, E. R. Mansell, and J. M. Straka, 2008: Numerical simulations of the electrification and microphysics of the weakly electrified 9 February 1993 TOGA COARE squall line: Comparisons with observations. *Mon. Wea. Rev.,* **136,** 364–379, doi:10.1175/2007MWR2156.1.

——, R. F. Rogers, F. D. Marks, and D. S. Nolan, 2009: The impact of horizontal grid spacing on the microphysical and kinematic structures of strong tropical cyclones simulated with the WRF-ARW model. *Mon. Wea. Rev.,* **137,** 3717–3743, doi:10.1175/2009MWR2946.1.

——, E. R. Mansell, C. L. Ziegler, and D. R. MacGorman, 2012: Application of a lightning data assimilation technique in the WRF-ARW model at cloud-resolving scales for the tornado outbreak of 24 May 2011. *Mon. Wea. Rev.,* **140,** 2609–2627, doi:10.1175/MWR-D-11-00299.1.

——, J. Gao, C. L. Ziegler, E. R. Mansell, D. R. MacGorman, and S. R. Dembek, 2014: Evaluation of a cloud-scale lightning data assimilation technique and a 3DVAR method for the analysis and short-term forecast of the 29 June 2012 derecho event. *Mon. Wea. Rev.,* **142,** 183–202, doi:10.1175/MWR-D-13-00142.1.

Fritsch, J. M., and C. F. Chappell, 1981: Preliminary numerical tests of the modification of mesoscale convective systems. *J. Appl. Meteor.,* **20,** 910–921, doi:10.1175/1520-0450(1981)020<0910:PNTOTM>2.0.CO;2.

Gallus, W. A., Jr., and M. Segal, 2001: Impact of improved initialization of mesoscale features on convective system rainfall in 10-km Eta simulations. *Wea. Forecasting,* **16,** 680–696, doi:10.1175/1520-0434(2001)016<0680:IOIIOM>2.0.CO;2.

Gandin, L. S., and A. H. Murphy, 1992: Equitable skill scores for categorical forecasts. *Mon. Wea. Rev.,* **120,** 361–370, doi:10.1175/1520-0493(1992)120<0361:ESSFCF>2.0.CO;2.

Goodman, S. J., and Coauthors, 2013: The GOES-R Geostationary Lightning Mapper (GLM). *Atmos. Res.,* **125–126,** 34–49, doi:10.1016/j.atmosres.2013.01.006.

Hamill, T. M., 1999: Hypothesis tests for evaluating numerical precipitation forecasts. *Wea. Forecasting,* **14,** 155–167, doi:10.1175/1520-0434(1999)014<0155:HTFENP>2.0.CO;2.

Hong, S.-Y., and J.-O. J. Lim, 2006: The WRF single-moment microphysics scheme (WSM6). *J. Korean Meteor. Soc.,* **42,** 129–151.

Hu, M., M. Xue, and K. Brewster, 2006: 3DVAR and cloud analysis with WSR-88D level-II data for the prediction of the Fort Worth, Texas, tornadic thunderstorms. Part I: Cloud analysis and its impact. *Mon. Wea. Rev.,* **134,** 675–698, doi:10.1175/MWR3092.1.

Iacono, M. J., E. J. Mlawer, S. A. Clough, and J.-J. Morcrette, 2000: Impact of an improved longwave radiation model, RRTM, on the energy budget and thermodynamic properties of the NCAR community climate model, CCM3. *J. Geophys. Res.,* **105,** 14 873–14 890, doi:10.1029/2000JD900091.

Janjić, Z. I., 1994: The step-mountain eta coordinate model: Further developments of the convection, viscous sublayer, and turbulence closure schemes. *Mon. Wea. Rev.,* **122,** 927–945, doi:10.1175/1520-0493(1994)122<0927:TSMECM>2.0.CO;2.

Jones, C. D., and B. Macpherson, 1997: A latent heat nudging scheme for the assimilation of precipitation data into an operational mesoscale model. *Meteor. Appl.,* **4,** 269–277, doi:10.1017/S1350482797000522.

Kain, J. S., and J. M. Fritsch, 1993: Convective parameterization for mesoscale models: The Kain–Fritsch scheme. *The Representation of Cumulus Convection in Numerical Models, Meteor. Monogr.,* No. 46, Amer. Meteor. Soc., 165–170.

Kasahara, A., R. C. Balgovind, and B. B. Katz, 1988: Use of satellite radiometric imagery data for improvement in the analysis of divergent wind in the tropics. *Mon. Wea. Rev.,* **116,** 866–883, doi:10.1175/1520-0493(1988)116<0866:UOSRID>2.0.CO;2.

Klemp, J. B., and R. B. Wilhelmson, 1978: The simulation of three-dimensional convective storm dynamics. *J. Atmos. Sci.,* **35,** 1070–1096, doi:10.1175/1520-0469(1978)035<1070:TSOTDC>2.0.CO;2.

Krishnamurti, T. N., J. Xue, H. S. Bedi, K. Ingles, and O. Oosterhof, 1991: Physical initialization for numerical weather prediction over the tropics. *Tellus,* **43A,** 53–81, doi:10.1034/j.1600-0870.1991.t01-3-00007.x.

Kuhlman, K. M., C. L. Ziegler, E. R. Mansell, D. R. MacGorman, and J. M. Straka, 2006: Numerically simulated electrification and lightning of the 29 June 2000 STEPS supercell storm. *Mon. Wea. Rev.,* **134,** 2734–2757, doi:10.1175/MWR3217.1.

Lericos, T. P., H. E. Fuelberg, M. L. Weisman, and A. I. Watson, 2007: Numerical simulations of the effects of coastlines on the evolution of strong, long-lived squall lines. *Mon. Wea. Rev.,* **135,** 1710–1731, doi:10.1175/MWR3381.1.

Lin, Y., and K. E. Mitchell, 2005: The NCEP stage II/IV hourly precipitation analyses: Development and applications. Preprints, *19th Conf. on Hydrology,* San Diego, CA, Amer. Meteor. Soc., 1.2. [Available online at http://ams.confex.com/ams/pdfpapers/83847.pdf.]

Loftus, A. M., D. B. Weber, and C. A. Doswell III, 2008: Parameterized mesoscale forcing mechanisms for initiating numerically simulated isolated multicellular convection. *Mon. Wea. Rev.,* **136,** 2408–2421, doi:10.1175/2007MWR2133.1.

Lopez, P., 2011: Direct 4D-Var assimilation of NCEP stage IV radar and gauge precipitation data at ECMWF. *Mon. Wea. Rev.,* **139,** 2098–2116, doi:10.1175/2010MWR3565.1.

Lynn, B. H., G. Kelman, and G. Ellrod, 2014: An evaluation of the efficacy of using observed lightning to improve convective lightning forecasts. *Wea. Forecasting,* in press.

Mahfouf, J.-F., P. Bauer, and V. Marécal, 2005: The assimilation of SSM/I and TMI rainfall rates in the ECMWF 4D-Var system. *Quart. J. Roy. Meteor. Soc.,* **131,** 437–458, doi:10.1256/qj.04.17.

Manobianco, J., S. Koch, V. M. Karyampudi, and A. J. Negri, 1994: The impact of assimilating satellite-derived precipitation rates on numerical simulations of the ERICA IOP 4 cyclone. *Mon. Wea. Rev.,* **122,** 341–365, doi:10.1175/1520-0493(1994)122<0341:TIOASD>2.0.CO;2.

Mansell, E. R., 2014: Storm-scale ensemble Kalman filter assimilation of total lightning flash-extent data. *Mon. Wea. Rev.,* **142,** 3654–3666, doi:10.1175/MWR-D-14-00061.1.

——, D. R. MacGorman, C. L. Ziegler, and J. M. Straka, 2005: Charge structure and lightning sensitivity in a simulated multicell thunderstorm. *J. Geophys. Res.,* **110,** D12101, doi:10.1029/2004JD005287.

——, C. L. Ziegler, and D. R. MacGorman, 2007: A lightning data assimilation technique for mesoscale forecast models. *Mon. Wea. Rev.,* **135,** 1732–1748, doi:10.1175/MWR3387.1.

Marecal, V., and J.-F. Mahfouf, 2003: Experiments on 4DVAR assimilation of rainfall data using an incremental formulation. *Quart. J. Roy. Meteor. Soc.,* **129,** 3137–3160, doi:10.1256/qj.02.120.

Markowski, P. M., and Y. P. Richardson, 2010: *Mesoscale Meteorology in Midlatitudes*. Wiley-Blackwell, 430 pp.

McCaul, E. W., Jr., S. J. Goodman, K. M. LaCasse, and D. J. Cecil, 2009: Forecasting lightning threat using cloud-resolving model simulations. *Wea. Forecasting,* **24,** 709–729, doi:10.1175/2008WAF2222152.1.

McFarquhar, G. M., H. Zhang, G. Heymsfield, R. Hood, J. Dudhia, J. B. Halverson, and F. Marks, 2006: Factors affecting the evolution of Hurricane Erin (2001) and the distributions of hydrometeors: Role of microphysical processes. *J. Atmos. Sci.,* **63,** 127–150, doi:10.1175/JAS3590.1.

Mittermaier, M. P., and N. Roberts, 2010: Intercomparison of spatial forecast verification methods: Identifying skillful spatial scales using the fractions skill score. *Wea. Forecasting,* **25,** 343–354, doi:10.1175/2009WAF2222260.1.

Mlawer, E. J., S. J. Taubman, P. D. Brown, M. J. Iacono, and S. A. Clough, 1997: Radiative transfer for inhomogeneous atmosphere: RRTM, a validated correlated-k model for the longwave. *J. Geophys. Res.,* **102,** 16 663–16 682, doi:10.1029/97JD00237.

Naylor, J., and M. S. Gilmore, 2012: Convective initiation in an idealized cloud model using an updraft nudging technique. *Mon. Wea. Rev.,* **140,** 3699–3705, doi:10.1175/MWR-D-12-00163.1.

Papadopoulos, A., T. G. Chronis, and E. N. Anagnostou, 2005: Improving convective precipitation forecasting through assimilation of regional lightning measurements in a mesoscale model. *Mon. Wea. Rev.,* **133,** 1961–1977, doi:10.1175/MWR2957.1.

Park, S. K., and D. Zupanski, 2003: Four-dimensional variational data assimilation for mesoscale and storm-scale applications. *Meteor. Atmos. Phys.,* **82,** 173–208, doi:10.1007/s00703-001-0586-7.

Pessi, A. T., and S. Businger, 2009a: Relationships between lightning, precipitation, and hydrometeor characteristics over the North Pacific Ocean. *J. Appl. Meteor. Climatol.,* **48,** 833–848, doi:10.1175/2008JAMC1817.1.

——, and ——, 2009b: The impact of lightning data assimilation on a winter storm simulation over the North Pacific Ocean. *Mon. Wea. Rev.,* **137,** 3177–3195, doi:10.1175/2009MWR2765.1.

Petersen, W. A., H. J. Christian, and S. A. Rutledge, 2005: TRMM observations of the global relationship between ice water content and lightning. *Geophys. Res. Lett.,* **32,** L14819,doi:10.1029/2005GL023236.

Pickering, K. E., Y. Wang, W.-K. Tao, C. Price, and J.-F. Müller, 1998: Vertical distributions of lightning NOx for use in regional and global chemical transport models. *J. Geophys. Res.,* **103,** 31 203–31 216, doi:10.1029/98JD02651.

Price, C., and D. Rind, 1992: A simple lightning parameterization for calculating global lightning distributions. *J. Geophys. Res.,* **97,** 9919–9933, doi:10.1029/92JD00719.

Roberts, N. M., 2005: An investigation of the ability of a storm scale configuration of the Met Office NWP model to predict flood-producing rainfall. Met Office Tech. Rep. 455, 80 pp.

——, and H. W. Lean, 2008: Scale-selective verification of rainfall accumulations from high-resolution forecasts of convective events. *Mon. Wea. Rev.,* **136,** 78–97, doi:10.1175/2007MWR2123.1.

Rogers, R. F., J. M. Fritsch, and W. C. Lambert, 2000: A simple technique for using radar data in the dynamic initialization of a mesoscale model. *Mon. Wea. Rev.,* **128,** 2560–2574, doi:10.1175/1520-0493(2000)128<2560:ASTFUR>2.0.CO;2.

Rudlosky, S. D., and H. E. Fuelberg, 2013: Documenting storm severity in the mid-Atlantic region using lightning and radar information. *Mon. Wea. Rev.,* **141,** 3186–3202, doi:10.1175/MWR-D-12-00287.1.

Saunders, C. P. R., 1993: A review of thunderstorm electrification processes. *J. Appl. Meteor.,* **32,** 642–655, doi:10.1175/1520-0450(1993)032<0642:AROTEP>2.0.CO;2.

Schaefer, J. T., 1990: The critical success index as an indicator of warning skill. *Wea. Forecasting,* **5,** 570–575, doi:10.1175/1520-0434(1990)005<0570:TCSIAA>2.0.CO;2.

Schultz, C. J., W. A. Petersen, and L. D. Carey, 2011: Lightning and severe weather: A comparison between total and cloud-to-ground lightning trends. *Wea. Forecasting,* **26,** 744–755, doi:10.1175/WAF-D-10-05026.1.

Schwartz, C. S., and Coauthors, 2009: Next-day convection-allowing WRF model guidance: A second look at 2-km versus 4-km grid spacing. *Mon. Wea. Rev.,* **137,** 3351–3372, doi:10.1175/2009MWR2924.1.

Skamarock, W. C., and J. B. Klemp, 2008: A time-split nonhydrostatic atmospheric model for research and NWP applications. *J. Comput. Phys.,* **227,** 3465–3485, doi:10.1016/j.jcp.2007.01.037.

Snyder, C., and F. Zhang, 2003: Assimilation of simulated Doppler radar observations with an ensemble Kalman filter. *Mon. Wea. Rev.,* **131,** 1663–1677, doi:10.1175//2555.1.

Stauffer, D. R., and N. L. Seaman, 1990: Use of four-dimensional data assimilation in a limited-area mesoscale model. Part I: Experiments with synoptic-scale data. *Mon. Wea. Rev.,* **118,** 1250–1277, doi:10.1175/1520-0493(1990)118<1250:UOFDDA>2.0.CO;2.

Takahashi, T., 1978: Riming electrification as a charge generation mechanism in thunderstorms. *J. Atmos. Sci.,* **35,** 1536–1548, doi:10.1175/1520-0469(1978)035<1536:REAACG>2.0.CO;2.

Vonnegut, B., 1963: Some facts and speculations concerning the origin and role of thunderstorm electricity. *Severe Local Storms, Meteor. Monogr.,* No. 27, Amer. Meteor. Soc., 224–241.

Wang, H., J. Sun, S. Fan, and X.-Y. Huang, 2013: Indirect assimilation of radar reflectivity with WRF 3D-Var and its impact on prediction of four summertime convective events. *J. Appl. Meteor. Climatol.,* **52,** 889–902, doi:10.1175/JAMC-D-12-0120.1.

Weygandt, S. S., S. G. Benjamin, M. Hu, T. G. Smirnova, and J. M. Brown, 2008: Use of lightning data to enhance radar assimilation within the RUC and Rapid Refresh models. *Third Conf. on Meteorological Application of Lightning Data,* New Orleans, LA, Amer. Meteor. Soc., 8.4. [Available online at http://ams.confex.com/ams/pdfpapers/134112.pdf.]

Whitaker, J. S., and T. M. Hamill, 2002: Ensemble data assimilation without perturbed observations. *Mon. Wea. Rev.,* **130,** 1913–1924, doi:10.1175/1520-0493(2002)130<1913:EDAWPO>2.0.CO;2.

Wilks, D. S., 1995: *Statistical Methods in the Atmospheric Sciences.* Academic Press, 467 pp.

Xiao, Q., and J. Sun, 2007: Multiple-radar data assimilation and short-range quantitative precipitation forecasting of a squall line observed during IHOP_2002. *Mon. Wea. Rev.,* **135,** 3381–3404, doi:10.1175/MWR3471.1.